Characterization of the neutron beam at NEAR Station at n_TOF/CERN

Author:
Styliani GOULA

Academic Advisor:
Nikolaos PATRONIS

Department of Physics
UNIVERSITY OF IOANNINA

A dissertation submitted to the University of Ioannina
in accordance with the requirements of the degree of
MASTERS in the Faculty of Physics.

APRIL 2022

ABSTRACT

The *Time-Of-Flight* facility at CERN has yielded a plethora of high precision data since its establishment, thanks to the facility's infrastructure and state-of-the-art apparatuses. Throughout the second Long Shutdown (2019-2021), when the lead target was replaced with a nitrogen-cooled one, a new experimental area, the NEAR Station, was also manufactured in a close geometry to the spallation target. The NEAR's Station envision is to take advantage of the high neutron flux, at such a close distance to the target, to perform Maxwellian Average Cross-Sections measurements (MACS) fundamental to the nuclear astrophysics field, as well as for other measurements in terms of cross-sections determinations or even measurements related to nuclear technology. Although extensive modeling using various software tools has been performed to extract the properties of the NEAR's beam, experimental characterization in terms of flux and energy distribution is urgent. For this reason, a multi-foil activation campaign has been scheduled. Within this thesis, the preparation and performance of the first multi-foil activation experiment, along with some preliminary results will be presented. Multiple foils of gold, cadmium, nickel, bismuth, cobalt, indium, aluminium, scandium, and tungsten were irradiated for almost three weeks. Given that the neutron energy spectrum at n_TOF stretches eleven orders of magnitude, the choice of the reference reactions has been made according to their excitation function dependency on neutron energy as well as the produced radionuclide half-lives. Six neutron capture reactions were utilized for the determination of the neutron beam in the thermal and epithermal energy regions along with eleven threshold reactions for the fast energy region. The induced activities of the samples were measured using a 26% relative efficiency HPGe detector according to the measurement plan presented in this work.

Acknowledgments

First and foremost, I would like to express my gratitude to my supervisor, Dr. Nikolas Patronis, for his outstanding assistance during this project. It was an honor to be a part of his team. I would also like to thank Maria-Elisso Stamati and Efstathia Georgali, two of my coworkers who were eager to assist me. Maria Peoviti and Zinovia Eleme, two good friends and colleagues, deserve particular appreciation for the innumerable discussions, laughs, and ideas they shared with me along this journey. My friends deserve my deepest appreciation for supporting me in focusing on what was most essential. I can not forget to thank all of the working group with which I cooperated. Thanks in particular to PhD candidate Sotiris Chasapoglou and Post doc Researcher Veatriki Michalopoulou of the National Technical University of Athens for their assistance on several occasions during the experimental phase.

Dedication

To my family.

Finally, I wanted to express my appreciation to my family for simply being there for me. It may appear simple, yet it is the tiny things in life that give life meaning.
Thank you.

Styliani Goula
April 2022

TABLE OF CONTENTS

Page

LIST OF FIGURES

INTRODUCTION

From the beginning of the 21st century, the experimental field of neutron physics has engrossed its spotlight on Nuclear Astrophysics and Nuclear Technologies. Nuclear Astrophysics seeks to comprehend the nucleosynthesis of elements, which, beyond Fe, occurs predominantly through the slow (s-) and rapid (r-) neutron capture processes throughout star evolution [1]. In the field of Nuclear Technology, high precision data are of the highest importance for a wide range of studies in terms of fundamental and applied nuclear physics, advanced medical applications, nuclear reactors, as well as for the design and construction of accelerator-driven systems (ADS) [2].

From the nuclear physics field's discovery thus far, many experimental confirmations have been certified. More specifically, progress has been made in identifying experimental neutron-induced cross-sections, up-to-date data which are available online on nuclear databases such as ENDF [3], JENDL [4], JEFF [5], BROND [6], CENDL [7], TENDL [8], etc. All the libraries just mentioned deal with evaluated data. This means that these datasets are providing theoretical calculations which are being adjusted to data once they have first been validated experimentally. Nevertheless, in certain circumstances, experimental regions remain uninvestigated. This scarcity of experimental values leads to considerable inconsistencies amongst databases, which could be eliminated with the design and attainment of infrastructures that will allow extensive research.

For such high-quality measurements as well as for several other neutron-based applications, the incident particle flux must be determined with utmost caution and high-precision. As a corollary, a thorough understanding of *flux* is needed in terms of intensity and energy distribution, where

flux denotes the energy distribution of the total number of the incoming neutrons (measurement unit: n/cm^2/s) [9]. Furthermore, precise comprehension of fluxes at research premises is important for dosage estimation as well as in radiation damage studies [10].

The installation of the neutron *Time-Of-Flight* facility of the European Organization for Nuclear Research (**CERN**) is amongst the world's largest in neutron energy beamlines. Since its establishment in 2001, which was inspired by Prof. **Carlo Rubbia**'s idea [11], it has yielded a plethora of highly accurate data [12]. Even in complex physics cases, research has become possible due to the neutron facility's high luminosity, wide energy range and state-of-the-art detection and data collection equipment [13]. Despite the fact that the n_TOF's facility energy spectrum extends over eleven orders of magnitude (up to a few GeV), and thanks to the innovative facility's features, the monitoring of the neutron flux from a spallation source is challenging but feasible [14].
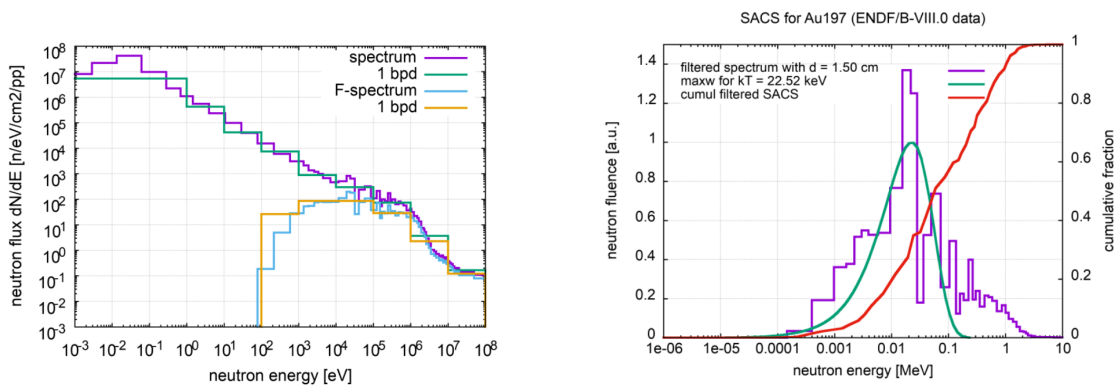
FIGURE 1.1. The neutron energy distribution is presented as a result of FLUKA simulations for different bin-width options without filters (pink and green lines) and with filters (blue and yellow). In the right figure, the filtered spectrum is shown (purple line) along with the Maxwellian distribution (green) for the temperature kT = 22.5 keV. [*Source*]

During CERN's Long Shutdown 2 phase (LS2), the n_TOF facility was greatly upgraded with radical innovations. The most important upgrade action was the installation of a new spallation target and the development of a new experimental area just outside the target bunker shielding. The motivation for the realization of the new experimental area, the NEAR station, is that the enhanced neutron flux close to the spallation target distances allows studies with minimal sample masses as well as the accurate determination of Maxwellian Averaged Cross-Sections (MACS) [14]. Even for highly radioactive samples becomes feasible by exploiting the high sensitivity and selectivity of the activation technique. Several simulations indicate that a Maxwellian-like neutron spectrum can be formed by adopting different filters configurations. For instance, Figure

1.1 demonstrates the shaping of the neutron beam energy distribution for a specific beam filter configuration.

Prior to the study and adoption of different filter configurations, it is very important to characterize the original NEAR neutron beam energy distribution. Accordingly, in the framework of the present thesis, the characterization of the NEAR experimental area was taken over. The necessary theoretical background for this work, and in particular, an overview of the generalized activation technique, is discussed in Chapter 1. The preparation of the first NEAR multi-foil activation measurement along with the preliminary calculations, the detector's calibration, and the gamma-ray measurements are then demonstrated in Chapter 2. Chapter 3 contains the data analysis using a 26% relative efficiency HPGe detector, accompanied by GEANT4 simulations to estimate the efficiency correction factor for gamma-attenuation [15]. Some preliminary experimental results are presented in Chapter 4. Finally, Chapter 5 consists of conclusions as well as a perspective for the newest experimental area at the n_TOF facility.

1.1 CERN's Accelerator Complex

The **C**onseil **E**oropéen pour la **R**echerche **N**ucléaire was established in 1954 with the vision of generating beamlines of diverse energies and intensities for several studies. As demonstrated in Figure 1.2, the beam is accelerated in stages and distributed accordingly, either to more powerful accelerators or to different experimental areas and facilities. The initial ion source provides negatively charged hydrogen ions (H^-) that are injected into *Linac4*, CERN's first linear accelerator. It measures 86 meters in length and is buried 12 meters underground, designed to accelerate negative hydrogen ions up to 160 MeV. Following this initial phase and during the particles' injection from *Linac4* into the *Proton Synchrotron Booster* (PSB) - a synchrotron consisting of four parallel rings - the two electrons of each ion are stripped, leaving behind hydrogen nuclei, protons. There, protons are accelerated up to 2 GeV. This proton beam is directed to the ***I**sotope mass **S**eparator **O**n**L**ine **DE**vice* (ISOLDE), where a sequence of processes results in a low-energy radioactive nuclide beam, utilized for astrophysics research, nuclear structure studies, material science, and medical applications. Continuing the beam's route from the PSB, it is infused into the *Proton Synchrotron* (PS). The PS, which has a circumference of 628 meters, operates at up to 26GeV and sends the beam directly to three experimental areas: the *Antiproton Decelerator* (AD) where antimatter studies are executed, the *neutron Time-Of-Flight* facility (n_TOF) for studying interactions between neutron and nucleus, and the *East Area* (EA) whereby, among others, are implemented and detector tests. Thereafter, the beam from the PS is being sent into the *Super Proton Synchrotron* (SPS), a powerful accelerator where it can reach 450 GeV and is used for High Energy Particle Physics research. Following the SPS accelerator stage, the beam can be directed either to *North Area* (NA), or to the *Advanced Proton Driven Plasma*

Wakefield Acceleration Experiment (AWAKE) or, of course, to the *Large Hadron Collider* (LHC)·
the most powerful accelerator-collider in the world with four different experiments running in
parallel.
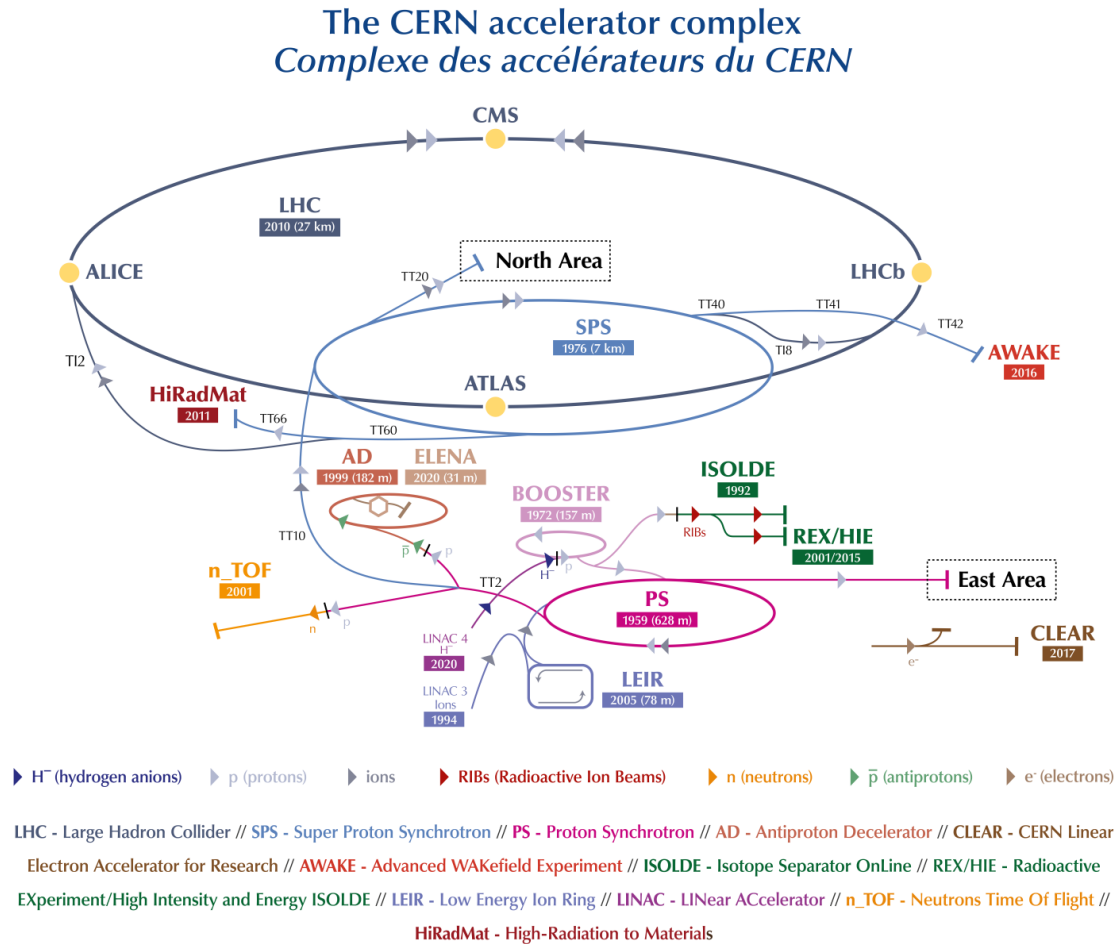
FIGURE 1.2. Overview of CERN's accelerator complex.

1.1.1 The *Time-Of-Flight* facility

The n_TOF facility at CERN is a *Time-Of-Flight* facility. The facility's name stems from the
process by which neutron energies are determined· based on the time-of-flight from the spallation
target to detector. It is designed to investigate neutron-nucleus interactions with applications in
fundamental science, nuclear astrophysics, nuclear technology, as well as in advanced nuclear
medicine research [9]. At the n_TOF facility, neutron beams are generated when a pulsed proton
beam with a momentum of 20 GeV/c, impinges on the lead spallation target. The time-width of
the proton pulse is 7 ns (sigma) and the nominal intensity is 7E+12 protons. The pulse repetition

rate is low enough ($\leq$ 0.8 Hz) to avoid possible sub-thermal and high-energy neutrons overlap between sequential pulses. When protons hit the target, high-energy neutrons are produced through spallation [16]. The produced neutrons are undergoing a stochastic route inside the lead target material due to the multiple scattering process. For this reason the final neutron beam energy distribution covers a huge energy range of more than eleven orders of magnitude neutron energies (meV - GeV). As shown in Figure 1.3 two flight paths under high vacuum have been constructed and are functional.

Throughout its first two operational phases, one flight line was employed at n_TOF, which is guided to Experimental ARea 1 (EAR-1). EAR-1 is located at the end of an almost horizontal flight path with a slight inclination of 185m in length. The neutron beam in this area is characterized by its high instantaneous intensity and high energy resolution, making it suitable for high-resolution measurements of neutron capture processes on stable or long-lived radioactive isotopes [17]. Amidst this, an additional vertical flight path of 20m was fabricated from the outset of the third phase in 2014, which led to Experimental ARea 2 (EAR-2). EAR-2 has higher neutron flux specifications since the flight path is significantly shorter. This enables the experimental area to be appropriate for the realization of measurements on radioisotopes with short half-lives, minimal sample masses and/or the study of low cross-sections' reactions [18].
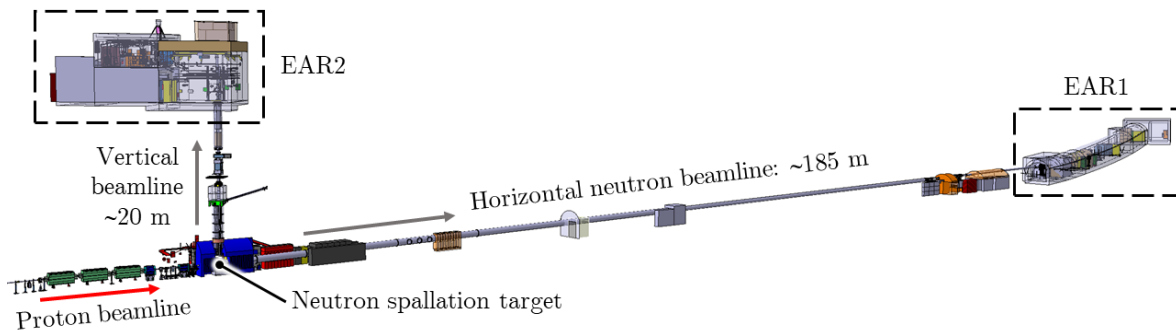
FIGURE 1.3. The flight path to n_TOF's experimental areas.

During the LS2, 2019-2021, the replacement of the lead spallation target (target #2) with a new nitrogen-cooled one (target #3) was completed [19], and the NEAR Station was established in a close range· approximately 3 meters away from the spallation target, sightly out of the shielding wall [20]. A collimating system is used to shape the neutron beam through an aperture. To attenuate the high-energy neutrons, the shielding wall consists of 40 cm of steel, 80 cm of concrete, and 20 cm of marble (Fig. 1.4(a)). The experimental hall depicted in Figure 1.4 was designed based on a 3D model geometry with FLUKA Monte Carlo simulations [21] and accurately represents the experimental NEAR area. According to extended FLUKA simulations, the flat spatial beam

profile has a width of 5 cm (Fig. 1.5()) [22].
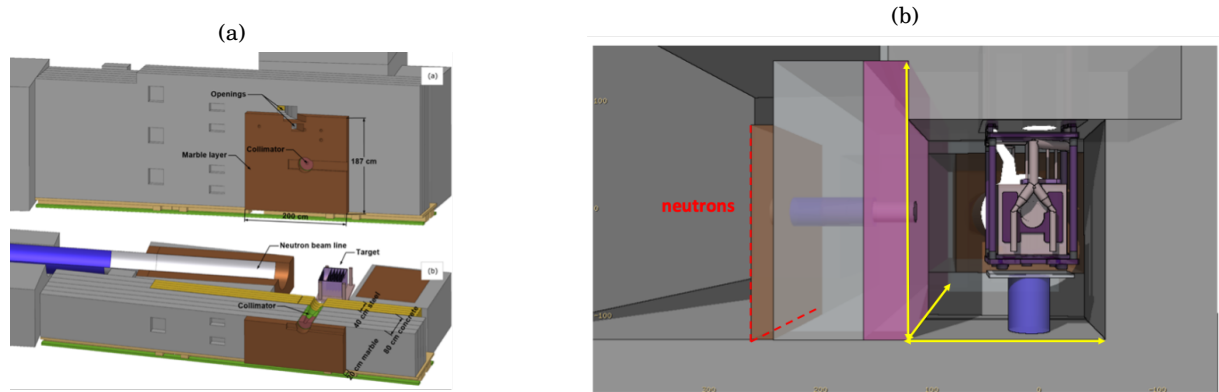
FIGURE 1.4. (a) The NEAR Station, and (b) the target on Fluka 3D model.

As this experimental zone is novel at the n_TOF facility, the neutron beam characteristics along with the energy distribution are, at the time being, unidentified. In order to accomplish the applied characterization procedure of the NEAR's beam, the multi-foil activation campaign was applied.
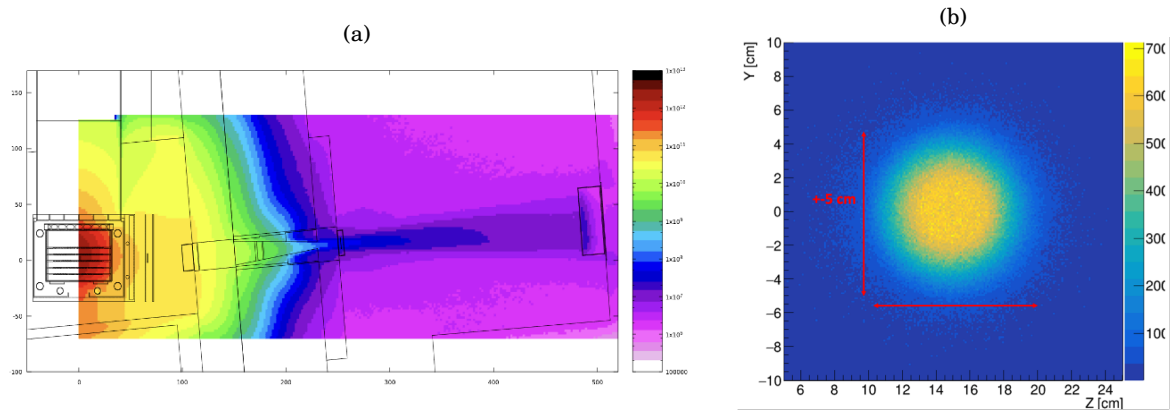
FIGURE 1.5. (a) The radiation at NEAR Station, and (b) the flat spatial profile of the NEAR's beam.

1.2 Nuclear Reactions

It might be useful to define the term "Q-value" before discussing excitation functions and neutron-nucleus interactions as well. The "Q-value" is the amount of energy released during a nuclear reaction, as calculated by the equation:

$$(1.1) \qquad Q = (m_{initial} - m_{final}) \, c^2$$

"Exothermic" reactions are those in which the *"Q-value"* is positive. The reaction is called *"endothermic"* when the *"Q-value"* is negative, and in these cases, the reaction can occur only if the available energy in the center-of-mass system is equal or higher than the absolute value of the *"Q-value"*.

1.2.1 Excitation functions

An excitation function is a representation of the cross-section dependence on the energy of the incoming particle. Specifically, for those nuclear reactions induced by neutrons, the absence of coulomb repulsion allows for interactions with the target nucleus even at zero kinetic energy. For the low-energy part, the total reaction cross-section's dependence on neutron energy is proportional to the inverse law of neutron's velocity, $\frac{1}{v_n}$. As the energy of the impinging neutron is increased, the total cross-section is reduced, while sharp peaks correspond to resonance peaks as caused by the available nuclear states in the compound nucleus (see Fig. 1.6).
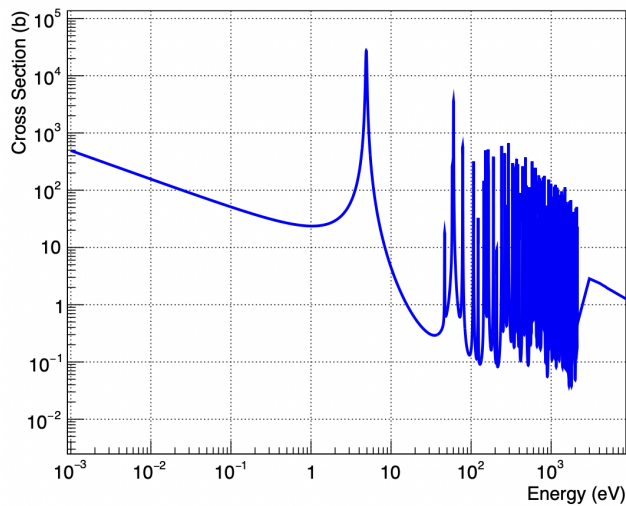
FIGURE 1.6. Excitation function of the ^{197}Au capture reaction.

The excitation functions of threshold reactions, in contrast to the capture reactions, as the energy of the projectile increases, there is an increase in the cross-section. As it is depicted in the following picture (see Fig. 1.7), the probability of a threshold reaction to take place is much lower than a low energy neutron capture reaction. At even higher energies, competing reaction

channels become important, and for this reason, the observed reaction cross-section values follow a rather smooth declining behavior after reaching a maximum value.
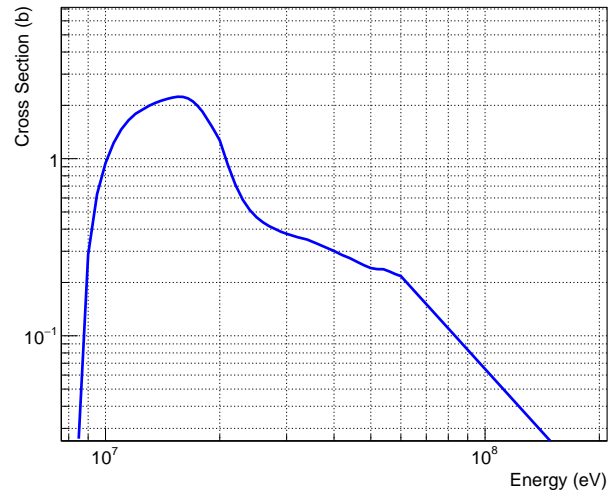
FIGURE 1.7. Excitation function of the ^{197}Au (n, 2n) reaction.

1.2.2 Neutron-Nucleus Interactions

Since the neutron has no charge, there is no Coulomb barrier to overcome when approaching the target-nucleus. It only interacts with it through the strong force. The interaction can take place in a variety of ways:

- **Elastic scattering**

  The process of elastic scattering occurs when a neutron interacts with the nucleus and the energy state of the nucleus remains unchanged. This procedure is frequently denoted by the abbreviation $(n,\ n)$ or $(n,\ elastic)$.

- **Inelastic scattering**

  This interaction is similar to the elastic process, with the only variation being the nucleus' final energy state. The neutron transfers energy to the nucleus, leaving it in an excited state. This process can be noted as $(n,\ n')$.

- **Capture reactions**

  The incoming neutron is absorbed by the nucleus in these processes, and gamma-radiation is emitted. It is an exothermic process since electromagnetic radiation is emitted, and it is

indicated as $(n, gamma)$.

- **Other reaction channels**
  The interaction of a neutron with the target-nucleus can cause the emission of charged particles (e.g. (n, α), (n, p), (n, d) reactions) or one or more neutrons $((n, xn)$ reactions). These reactions occur as compound nucleus reactions or as direct reactions, depending on the neutron energy. [23].

1.2.3 Types of Nuclear Reactions

Nuclear reactions can be divided into two major categories with respect the reaction mechanism: the compound nucleus reactions and the direct reactions.

1.2.3.1 Compound-nucleus reactions

Consider a neutron as a projectile, and a slower or stationary target-nucleus. Keeping in mind that the projectile is affected only from the strong nuclear force and according to Bohr's model, it interacts with target-nucleus as a whole and through multiple collisions the energy is spread throughout the nucleus. This kind of state is known as the compound nucleus, which may be expressed as:

$$\text{(1.2)} \qquad\qquad {}^{A}_{Z}\text{X} + {}^{1}_{0}\text{n} \rightarrow ({}^{A+1}_{Z}\text{X})^{*}$$

where ${}^{1}_{0}$n denotes the neutron, ${}^{A}_{Z}$X the target nuclei, X the chemical element, Z the number of protons, A the number of nucleons, and $({}^{A+1}_{Z}\text{X})^{*}$ the compound nucleus. These reactions consist of two stages: 1) the compound nucleus formation and 2) the de-excitation of it. The time scale of this type of nuclear reaction is of the order of 10^{-16} to 10^{-18} sec. The de-excitation is happening in an independent way from the formation of the compound nucleus, and it may happen with more than one decay pathway, as is shown in the Table 1.1, provided that are energetically allowed [24].

1.2.3.2 Direct reactions

The second type of reactions, as mentioned previously, are the direct reactions. In this case, the projectile collides with the nucleus' surface. This reaction mechanism becomes dominant at higher neutron beam energies. Thus, for 1 MeV energy of the incoming nucleon corresponds to a wavelength of 4 fm, and it is more probable to interact through a compound-nucleus reaction. 20 MeV incident energy, it corresponds to about 1 fm wavelength and the incident particle can participate in direct processes. The time duration of the direct reactions is much smaller than

Table 1.1: De-excitation pathways of a compound-nucleus.

Elastic scattering (n, n)	$(^{A+1}_{Z}X)^* \rightarrow {}^A_Z X + {}_0 n^1$
Inelastic scattering (n, n')	$(^{A+1}_{Z}X)^* \rightarrow {}^A_Z X + {}_0 n^1 + \gamma$
Radioactive capture (n, gamma)	$(^{A+1}_{Z}X)^* \rightarrow {}^A_Z X + \gamma$
(n, p) reaction	$(^{A+1}_{Z}X)^* \rightarrow {}^A_{Z-1} Y + {}^1_1 H$
(n, a) reaction	$(^{A+1}_{Z}X)^* \rightarrow {}^{A-3}_{Z-1} Y + {}^4_2 He$
(n, Xn) reactions	–

the compound-nucleus, in the order of 10^{-22} sec, by about equal to the time that is needed for an incident particle to cross the target nucleus [24].

1.3 Activation Technique

In comparison to other nuclear methods, the Activation Technique is a widespread technique that has been in use for many years and plays a leading role. The fundamental idea was utilized in 1936 by George Hevesy and his student Hidle Levi to determine the levels of dysprosium in a yttrium sample. This technique has applications in many scientific research fields, such as chemistry, archaeology, geology, nuclear physics, and nuclear medicine, among other scientific domains. The basic technique relies on the measurement of the radiation emitted by artificial radionuclides which were formed after the material's irradiation. More specifically, the activation technique is comprised of two steps:

- The first step is to irradiate a well-known amount of material using a particle beam to produce unstable nuclei with appropriate decay parameters. [1]

- The induced activity must then be quantified as a second step.

The general equation of the activation technique is:

$$(1.3) \qquad \sigma = \frac{counts\ CF}{N_T\ \Phi\ \varepsilon\ I_\gamma\ (1 - e^{-\lambda t_m})\ e^{-\lambda t_w}\ f_b},$$

where counts represent the photopeak's net counts, CF the correction factors as self-attenuation,

---

[1] The proper irradiation time depends on the radioactive nucleus' half-life.

detector's dead time, etc., Φ the total beam flux, N_T the number of target-nuclei in the sample, I the intensity of the emitted gamma-ray, ε the detector's efficiency for the energy of the emitted gamma-ray, λ the decay constant of the product nucleus, t_m the measuring time of the induced activity, t_w the waiting time between the end of the irradiation and the start of measurement, and f_b the correction factor for the activated nuclei decay during the irradiation, where

- for constant flux

$$(1.4) \qquad f_b = \frac{1 - e^{-\lambda t_{irr}}}{\lambda t_{irr}}$$

- for non-constant flux

$$(1.5) \qquad f_b = \frac{\int_0^{t_{irr}} f(t)\, e^{\lambda t}\, dt}{\int_0^{t_{irr}} f(t)\, dt}\, e^{-\lambda t_{irr}}$$

The neutron flux and the activation rate are related to each other in the following way:

$$(1.6) \qquad R = N_T \int_E \sigma(E)\, \Phi(E)\, dE\ \ f_b,$$

with the number of the target-nuclei given by:

$$(1.7) \qquad N_T = \frac{m\, a\, N_A}{MW},$$

where N_T represents the number of the target-nuclei, m is the mass of the sample, α the abundance of isotope, σ the cross-section for the reaction, N_A the Avogadro's Number, and MW the molecular weight. A more detailed description is given in the Appendix A.

In principle, as can be seen in Table 1.2, the activation equation (Eq. 1.6) can be used for different purposes, depending on the application. The technique can be used to determine the reaction cross-section when the mass of the sample and the neutron flux are known. Alternatively, if the reaction cross-section is known, the activation technique can be used for the determination of the neutron flux.

A graphical representation of the technique, considering for instance the study of a neutron capture reaction, is given in Figure 1.8. Projectiles - in this case, neutrons - are impinging on a stable target-nucleus, resulting in the production of radioactive nuclei. The incoming neutron

Table 1.2: The following are the three quantities of Eq. 1.6: flux, cross-section and number of nuclei. If the two quantities are known, the third can be determined.

Cross-Section	Flux	N_T
√	√	Could be determined
√	Could be determined	√
Could be determined	√	√

enters the target-nucleus and, through collisions, transfers all of its energy (plus the separation neutron energy) to the nucleons. This process leads to a compound nucleus excited state, in which, the identity of the particle that caused the excitation is lost. The excitation energy determines the manner in which the compound nucleus is de-excited, despite the fact that it is unaffected by the producing process.
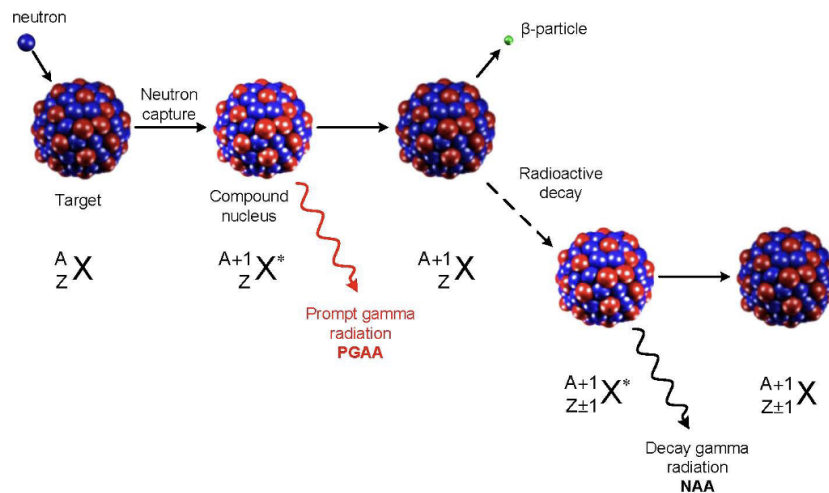
FIGURE 1.8. Graphic representation of the Neutron Activation Analysis method.

The compound nucleus de-excites in a variety of ways. The simplest of these is to instantly release one or more gamma-rays. Other more complicated modes of de-excitation can occur in instances where adequate excitation energy is available. In these modes of de-excitation, one or more particles can be emitted from the highly excited compound nucleus. The producted nucleus can be either stable or unstable. For the reactions that lead to unstable product nuclei, the activation technique can be utilized if the decay characteristics allow it [25].

Like any technique, the activation technique has some limitations. In order to be able to apply the technique, certain requirements must be met. The most critical parameter that defines its applicability is the half-life time of the product nucleus. The activation technique makes it difficult to study nuclear reactions in which the product nucleus has a very short or extremely

long half-life time. [26].

1.4   Semiconductor Detectors

The detection of particles and radiation in solid-state semiconductor detectors is based on the recording of the energy deposition of secondary particles, which are produced through the transportation of radiation in the detector material. The semiconductor detectors are actually inversely polarized diodes that convert the energy deposition of the impinging radiation into a proportional electric pulse. More specifically, the semiconducting material crystal, such as Si or Ge, contains well-defined atomic states that are arranged into bound energy levels. When ionizing radiation enters, creates an equal number of electrons and holes in the detector's semiconductive material. Electrons are free to move in the conduction band as they react with the electric field of the detector, and they are gathered at an electrode and converted into an electronic pulse that is sent to the pre-amplifier. Then, the signal is directed to the amplifier, where the final shaping and amplification stage takes place. Following the amplification and shaping of the initial pulse with well-defined characteristics, the digitization of the pulse is achieved through analog-to-digital converters (ADC). The recorded spectrum can be saved either in event-by-event mode or via the appropriate software/firmware multi-channel analyzer (MCA), where the full acquired spectrum is recorded (Fig. 1.9) [26].
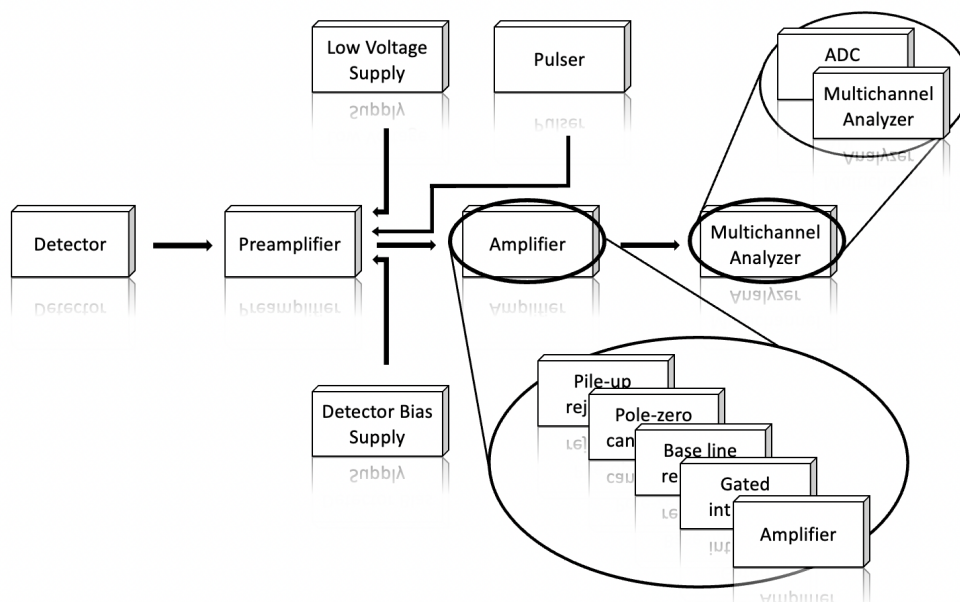
FIGURE 1.9. Electronic system for gamma-ray measurements.

1.4.1 Interaction of Electromagnetic radiation with matter

When gamma- and X- rays penetrate matter, inevitably they interact with it through various processes. The most important are the following three:

1. Photoelectric effect

2. Compton scattering

3. Pair production

1.4.1.1 Photoelectric effect

The photoelectric effect is the absorption of a photon when it interacts with a bound electron (see Fig. 1.10). As a result, the electron is ejected, known as photoelectron, which has kinetic energy:

$$E_e = E_g - E_b,$$

(1.8)

where E_e represents the energy of the released electron, E_g the gamma-ray energy, and E_b the electron's binding energy. The energy of the released electron depends on the photon's energy. So, after this interaction, the atom is in an excited state and returns to its ground state through one of the two following ways:

- the atom's de-excitation through the energy's redistribution, or

- the vacancy which has been left due to the emitted photoelectron is occupied by an electron with higher energy.

The first case results in the emission of more electrons, a process known as Auger cascade, while the second results in the emission of a photon in the X-ray energy range [27].

1.4.1.2 Compton scattering

In the Compton effect, a photon is scattered by an electron, transferring only a portion of its energy. This results in a secondary photon lower in energy, and the photon's energy loss is transferred to the scattered electron (Fig. 1.11). Due to the energy's and momentum's conservation, the energy of the electron is given by the following formulas:

$$E_e = E_g - E'_g$$

(1.9)
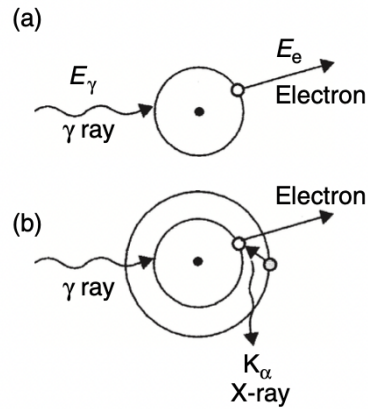
FIGURE 1.10. Schematic representation of photoelectric absorption, and (b) the transition of a K_a electron with simultaneous emission of X-rays.
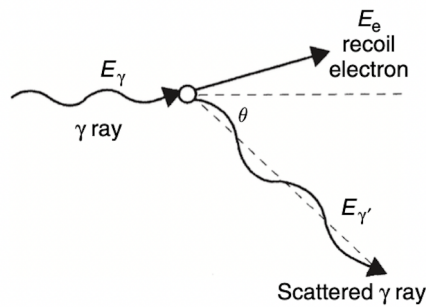
FIGURE 1.11. Schematic representation of Compton scattering mechanism.

or including angle θ:

$$(1.10) \qquad E_e = E_g \{ 1 - \frac{1}{([1 + E_g(1 - cos\theta)\frac{1}{(m_0 c^2)})} \},$$

where E_e represents the energy of the scattered electron, E_g the photon's energy, and E'_g the scattered photon's energy. The E_e is differing according to the various angles which the photon may be scattered. For the scattering angle of $\theta = 0$ °, no energy is transferred to the electron. So, the electron's energy is 0 and the scattered photon has the same energy as before the interaction. For the case of θ=180 °, the incident photon will give a large amount of energy to the recoil electron. For angles that are in the intermediate range of 0 ° $< \theta <$ 180 °, the energy and angle dependence is given in the following Figure 1.12 [27][28].

15
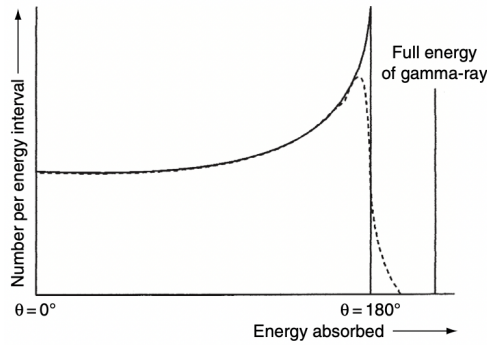
FIGURE 1.12. Transferred energy related to angle θ due to Compton scattering.

1.4.1.3 Pair production

For gamma-rays with higher energies, particularly in the MeV region, the dominant interaction mechanism seems to be pair production. During this process, a photon transforms to a positron-electron pair (Fig. 1.13). In order for this kind of interaction to be feasible , there is obviously a threshold of $2mc^2$. More concisely, the incident photon should have energy at least equal to the sum of the rest masses of the two particles, 511 keV each.
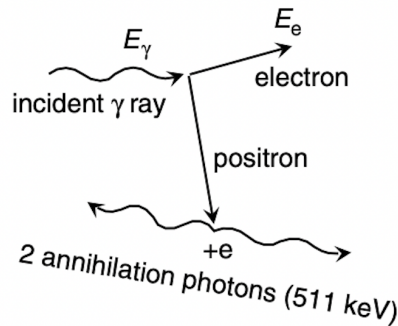
FIGURE 1.13. Schematic representation of pair production followed by positron's annihilation to two photons.

If the gamma-ray has energy greater than 1022 keV, the excess energy is shared between the electron-positron pair as follows:

$$(1.11) \qquad\qquad E_g = T_+ + mc^2 + T_- + mc^2,$$

16

where T_+ represents the positron's energy and T_- the electron's energy. When a photon interacts with matter, it does so through one of the three mechanisms mentioned above. Of course, there are more than these three ways for a photon to interact with matter, however, as long the gamma-ray detection is concerned the dominant interaction processes are these ones. Figure 1.14 shows the importance of three processes according to the incident photon energy with the number Z [27] [28] [29].
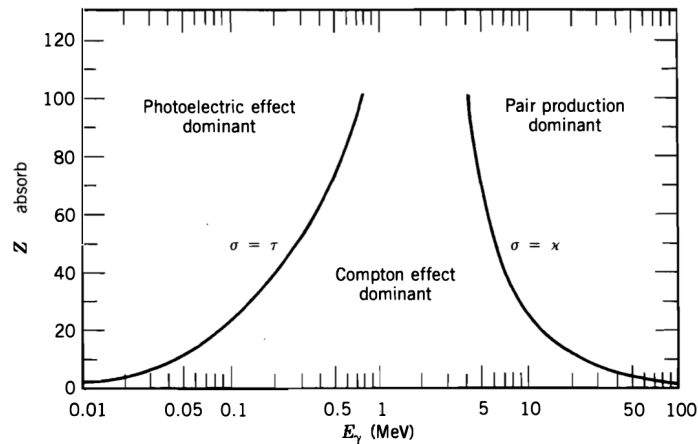
FIGURE 1.14. Importance of the three processes.

1.4.2 High Purity Germanium Detectors

The detector material is important and affects the characteristics and performance of the detector; not only is the type of material important, but so is the manufacturing and shaping of the semiconductor. Considering gamma-ray detection through semiconductor material, the germanium is promoted as the proper material since it detects highly penetrating gamma-rays and establishes full energy deposition in large volumes. The ability to create a large depleted region through inverse polarizing is strong limited by silicon detectors, but it is possible with High Purity Germanium detectors. Furthermore, the absorption coefficients for all the interaction processes increase relative to the atomic number, materials with high atomic numbers are preferred. In addition to all the benefits mentioned so far, the HPGe detectors are widely used owing to their excellent energy resolution.

Since the HPGe detectors are semiconductor detectors, the principle of operation is the same as that mentioned above: radiation enters the depletion region and creates electron-hole pairs. The strong electric field as formed in the depletion region drives the electrons towards to the anode of

the crystal and the holes towards to the cathode. In this way, the electrons can form an electric pulse whose amplitude is proportional to the total energy deposited in the germanium crystal's depleted region.

Efficiency ε

The absolute peak efficiency ε of a gamma-ray detector could be expressed as in Eq. 1.12 which indicates the ratio of the events recorded by the detector to those emitted by the source.

$$(1.12) \qquad \varepsilon = \frac{recorded\ photons}{photons\ emitted\ from\ the\ source}$$

The absolute peak efficiency can also be expressed as a product of the intrinsic efficiency ε_{ins} and the geometrical factor G, as given in the following equation.

$$\varepsilon = \varepsilon_{ins}\ G$$

$$(1.13) \qquad \varepsilon = \frac{recorded\ photons}{photons\ detected\ by\ the\ detector}\ \frac{\Delta\Omega}{4\pi}$$

Energy Resolution R

The energy resolution of a detector is its ability to distinct two rays with similar decay energies. Considering that the detection of a given gamma-ray with energy E, the resolution is:

$$(1.14) \qquad R = \frac{FWHM}{E},$$

where FWHM (Full Width at Half Maximum) represents the photopeak's width at the half of its height. Apparently, the lower the value the better the detector's ability to separate the gamma-rays.

Dead time

When a gamma-ray is recorded by full or partial energy deposition in the detector's active volume, an electrical pulse is created. Most data acquisition systems, cannot process other pulses for a given time interval while the pulse is being shaped and, more importantly, while the pulse height

is being digitized. This causes dead-time issues and, eventually, pulse losses. The problem of the dead time is no longer present in fully digital systems where the primary signal as comes from the detector pre-amplifiers is directly digitized through flash-ADC's, but pulses losses can still occur due to the probability of pulse pile-up [30].

1.5 Gamma-ray measurements

The NAA is one of the most sensitive and selective techniques for nuclear reaction cross-section measurements. The power of the NAA is based on the developments in the gamma-ray spectroscopy techniques. Despite the cutting-edge technology advances, there are plenty of difficulties that the researcher should take into consideration. Among them are interference reactions, contaminated peaks in the final spectrum, dead time during a measurement, shelf-shielding, coincidence-summing effects, etc.

1.5.1 Position of the samples

The detector's efficiency changes with respect to the source-to-detector-window distance according to the $\frac{1}{r^2}$ law. The adopted measurement geometry depends mostly on the sample characteristcs and most importantly on the expected activity. If one chooses to place the radioactive source at a small distance, it has some advantages, such as a high counting rate for a specific source, the possibility of using a smaller sample in terms of mass, and thus diminishing corrections related to attenuation, as well as decreasing the attenuation of the photons traveling within the air (<10keV). On the other hand, at a larger distance, there are plenty of advantages such as smaller coincidence-summing corrections, less sensitivity of the detection efficiency to small changes in the sample's shape and positioning, and smaller random-summing corrections for a given source activity [28].

1.5.2 Interference reactions

By applying the neutron activation technique, an interference reaction is a reaction in which the same product nuclei can be produced from different reaction channels. In these cases, the contribution of the different reaction channels to the formation of the product nucleus have to be carefully quantified. This is only possible when extensive experimental information is available for the competing reaction channels and if the neutron energy distribution is very well characterized.

1.5.3 Self-shielding

Another issue that could occur during the irradiation is the self-shielding. Self-shielding is the attenuation of the neutron beam within each sample itself because of the absorption of the

neutrons [23]. An example could be the Au sample, where the saturated resonance at 5 eV causes the strong attenuation of the neutron beam along the sample material. For this reason, the low energy neutron flux is not the same along the sample material and this phenomenon has to be taken into account.

1.6   Neutron Spectrum

The term *"neutron spectrum"* refers to the dependency of the neutron flux on the neutron energy. As it is depicted in the following Figure 1.15, the neutron energy spectrum can be divided into three parts corresponding to neutron energies: thermal, epithermal, and fast regions.
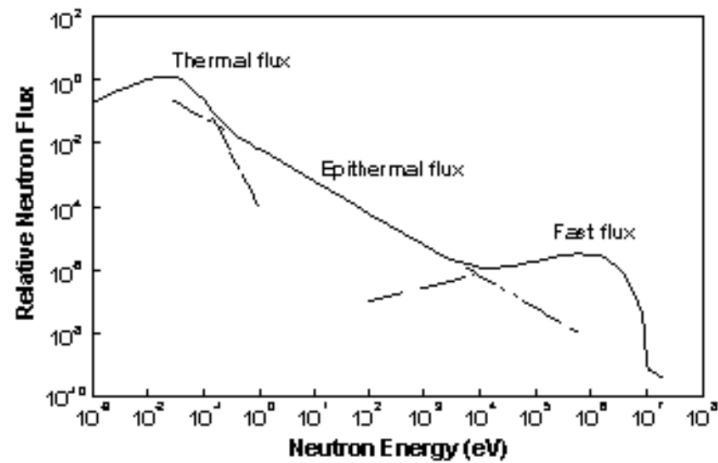
FIGURE 1.15. A typical neutron spectrum [31].

EXPERIMENTAL METHOD

The primary goal of this study is to characterize the NEAR beam's features by combining activity measurements of several samples through a multi-foil activation approach. Based on this method, natural samples in the form of foils with different threshold energies and excitation functions were irradiated for 22 days. Afterwards, the measurements of the sample's induced activity was performed by means of a High Purity Germanium detector (HPGe). The data acquisition time was carefully scheduled in order to obtain adequate statistics according to the half-live of each radionuclide.
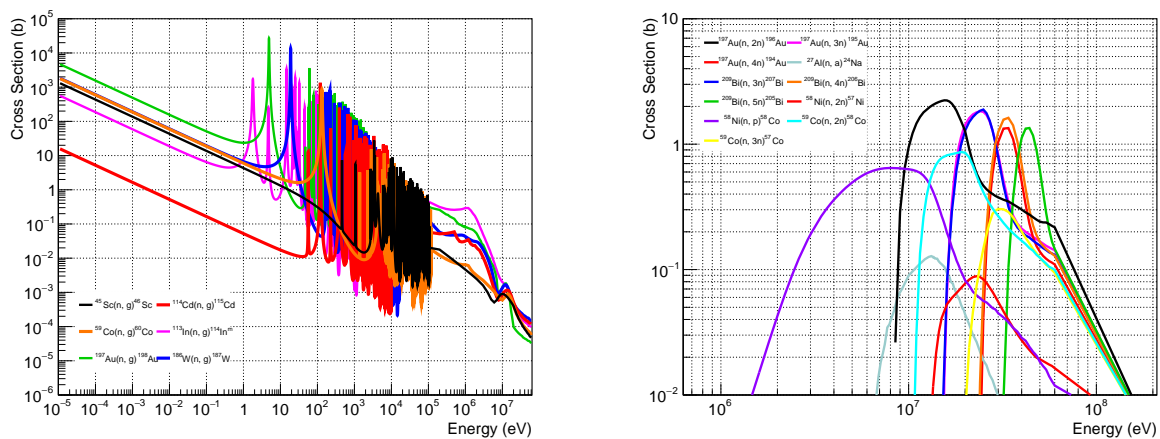
FIGURE 2.1. The high-precision cross-sections data as a function of incident neutron energy taken from TENDL s.60 Library.

Table 2.1: Chosen reactions under investigation.

Sample	Abundance	Reaction	Threshold [keV]	Eg [keV]	Intensity [%]	Half Life
Ni	0,68077	58Ni (n, p) 58Co	0	810,775	99,00	70.86 d
		58Ni (n, 2n) 57Ni	12429	1377,63	81,70	35.60 h
W	0,2843	186W (n, g) 187W	-	685,774	27,30	23.72 h
Al	1	27Al (n, a) 24Na	3250	1368.633	100,00	14.959 h
Cd	0,2873	114Cd (n, g) 115Cd	-	527,900	27,45	53.46 h
Bi	1	209Bi (n, 3n) 207Bi	14416	1063,662	74,50	31.55 y
		209Bi (n, 4n) 206Bi	22553	803,100	99,00	6.243 d
		209Bi (n, 5n) 205Bi	29622	1764,36	32,50	15.31 d
Au	1	197Au (n, g) 198Au	-	411,802	96,00	2.69517 d
		197Au (n, 2n) 196Au	8114	355,684	87,00	6.183 d
		197Au (n, 4n) 194Au	23260	328,455	61,00	38.02 h
In	0,0429	113In (n, g) 114In m	-	190,29	15,56	49.51 d
Sc	1	45Sc (n, g) 46Sc	-	1120,545	99,987	83.79 d
Co	1	59Co (n, g) 60Co	-	1332,501	99,9856	1925.34 d
		59Co (n, 2n) 58Co	10633	810,775	99,00	70.86 d
		59Co (n, 3n) 57Co	19353	122,0614	85,60	271.79 d

2.1 Experimental Set-up

For the experimental part of this study, a set of foils was chosen depending on the reaction cross-section and foil availability. Table 2.1, lists the 17 reference neutron-induced reactions under investigation, which comprise eleven threshold and six capture reactions. The reactions were chosen with care based on the excitation energies. The strong isolated resonances, as well as the different reaction thresholds, play an instrumental role in the unfolding procedure. This is a challenging undertaking given that the NEAR neutron energy spectrum ranges from the meV region up to GeV.

The cross-sections are known with sufficient precision and were acquired from the TENDL s.60 Library (see Fig. 2.1). As can be seen in the majority of the adopted capture reactions, there are strong resonances in the low neutron energies that allow mapping of this region, whereas for higher neutron energies, the different reaction thresholds can also serve the unfolding of the neutron energy spectrum in the MeV energy region.

2.1.1 The samples

The neutron activation technique can only be applied for reaction cross-section measurements or neutron beam characterization purposes if the sample mass and content are precisely known. Hand contact, for instance, can add a sufficient amount of salt to detect the presence of sodium and chloride (NaCl) in the samples that would subsequently be detected in the recorded spectrum. Thus, the surface of the samples was cleaned with ethanol before being placed in the holder. As illustrated in Figure 2.2, the masses of the samples were measured using a highly precise scaler and then placed in a container before being irradiated, in order to avoid accumulation of dust.
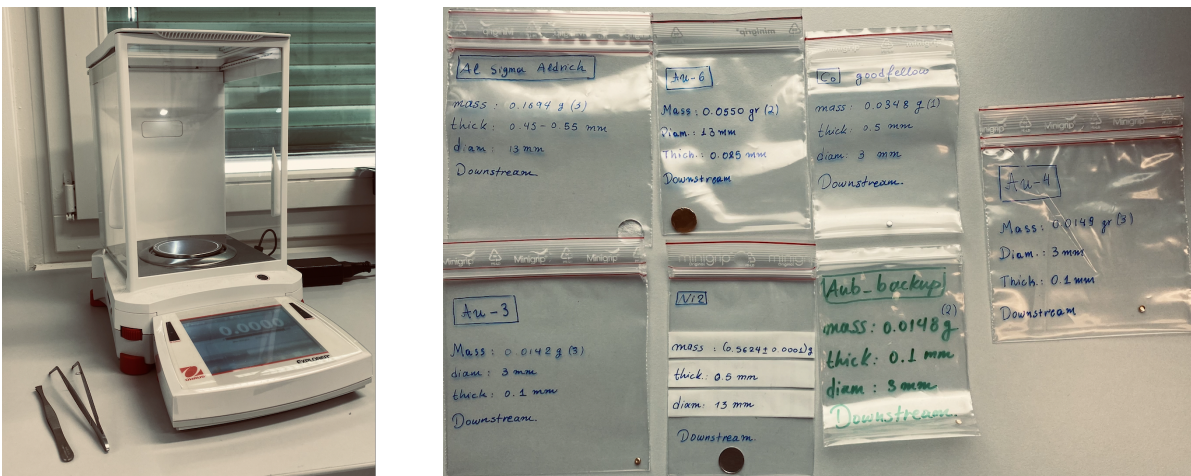
FIGURE 2.2. (a) The high precision scale and (b) the samples during the measurement process.

The samples along with the thicknesses, the diameters, the purity of the element, the mass, as well as the position in the holder (samples which were irradiated in the front and the back holder are upstream and downstream, respectively) are shown in the following Table 2.2. Small thicknesses were adopted in order to bound the impacts of self-shielding effects to a minimum at each foil.

Table 2.2: Specification and information about the samples used for the characterization of the neutron beam.

Sample ID	Thickness [mm]	Diameter [mm]	Purity [%]	Mass [gr]	Position
In-2	0.5	13	99,999	0,4675 ±0,0002	Upstream
Sc-GF	0.3	3	99	0,0073 ±0,0001	Upstream
W-3	0.5	12.7	>= 99,9	1,2349 ±0,0001	Upstream
Bi	1	13	99,999	1,1070 ±0,0003	Upstream

Cd	1	12.7	99,95	1,0714 ±0,0002	Upstream
Au-1	0.5	3	99,99	0,0709 ±0,0002	Upstream
Au-2	0.5	3	99,99	0,0712 ±0,0003	Upstream
Co-GF	0.5	3	99,99+	0,0348 ±0,0001	Downstream
Al-SA	0.45 - 0.55	13	99,999	0,1694 ±0,0003	Downstream
Ni-2	0.5	13	99,98	0,5624 ±0,0001	Downstream
Au-3	0.1	3	99,99	0,0142 ±0,0003	Downstream
Au-4	0.1	3	99,99	0,0149 ±0,0003	Downstream
Au-b	0.1	3	99,99	0,0148 ±0,0002	Downstream
Au-6	0.025	13	99,99	0,0550 ±0,0002	Downstream
Holder & Screws				38,4128 ±0,0002	

2.1.2 The irradiation set-up

Figure 2.3 depicts the configuration of the first Multi-foil Activation Measurement (MAM-1) in its final state. Depending on the reaction under examination, 9 samples could be placed in each holder, upstream and downstream for capture and threshold reactions, respectively. This is possible since the threshold reactions are unaffected by the presence of another sample in front of them. In this layout, a high-purity aluminum element was used to construct two identical holders and two hoops (Fig. 2.4). Each holder has a surface of $8 \ x \ 8 \ cm^2$ with 0.1 cm thickness. On this surface, there are apartures with 4 mm and 14 mm diameters for the samples' placement. Each of the hoops has an inner diameter of 4.98 cm. Within this diameter, samples with diameters of 3 mm and 13 mm and thicknesses ranging from 0.1 to 1 mm were positioned so as to be fully irradiated. The only exception in thicknesses was the Au-6 with 25 μm. The hoops along with eight screws were used to bolt the holders together. Pieces of mylar were employed to segregate the foils in distinct layers and avoid miss-placement during the irradiation. Figure 2.5 shows the holder during the alignment process, 20 cm away from the collimator exit.

2.2 Calculated Counting Rate & Expected Activity

Prior to the experiment, the counting rate of each reaction of interest was calculated in order to obtain adequate statistics and also to avoid issues related to radioprotection or excessive counting rates. For the accomplishment of the feasibility computations of each produced radionuclide, the National Nuclear Data Center, Brookhaven National Laboratory, USA (NNDC) data-base was utilized [32]. Specifically, for the reaction cross-sections the TENDL-2019 s.60 Library data-base was adopted while the gamma-ray energies, intensities, half-life times etc were taken from the NuDat library of NNDC. The expected activity of each foil is shown in the following Table 2.3. For those elements with more than one existing isotope in the sample, the isotopic abundance as well
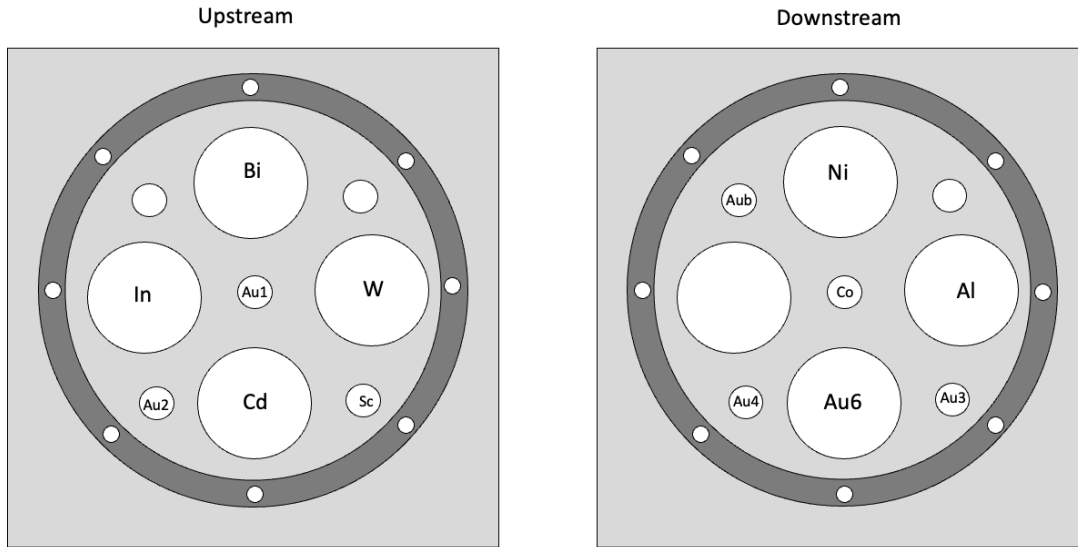
FIGURE 2.3. Arrangement of foils in the upstream and downstream holder.

as the "parasitic" reactions have been taken into account (e.g., (n, gamma)). For those physics cases in which more complicated phenomena existed (e.g., neutron self-attenuation), extensive GEANT4 simulations were performed for the accurate estimation of the expected activity of the samples.

It has to be noted that, the counting rate, and hence the expected activity, are calculated using the FLUKA-simulated neutron flux. During the estimation procedure, using the mean or the bin borders in order to draw conclusions about the spectrum-averaged cross-section (SACS) is imprecise. This is owing to the fact that the cross-section varies significantly along the bin width. To prevent such issues, a Monte Carlo method was developed and applied within the ROOT-based script written in the C++ language [33]. The sampling statistics (~1E4 events for each energy bin) were adjusted so as to have adequate sampling of the excitation function within each energy bin and, at the same time, reasonable CPU times have to be considered (see App. C).

Table 2.3: The induced activity of the samples after the irradiation. *(eoi)=end of irradiation, (a1d)=after 1 day, (a30d)=after 30 days.

Sample ID	Activity of foil (eoi)* [MBq]	Activity of foil (a1d)* [MBq]	Activity of foil (a30d)* [MBq]
Cd	2,1E-02	1,4E-02	2,5E-03
Sc	2,6E-04	2,6E-04	2,1E-04

Au-1	2,1E-01	1,6E-01	9,2E-05
Au-2	2,1E-01	1,6E-01	9,2E-05
Au-3	4,3E-02	3,2E-02	1,8E-05
Au-4	4,5E-02	3,4E-02	1,9E-05
Au-backup	4,5E-02	3,4E-02	1,9E-05
Au-6	1,5E-01	1,1E-01	6,7E-05
W	2,1E-01	1,0E-01	2,0E-03
In	3,3E-03	3,2E-03	2,2E-03
Ni	1,8E-03	1,5E-03	8,2E-04
Al	1,1E-03	1,4E-04	1,5E-18
Co	3,5E-04	1,9E-04	1,7E-04
Bi	1,2E-02	4,5E-03	5,2E-04
SUM	**9,6E-01**	**6,6E-01**	**8,6E-03**
Al Holder	2,6E-01	3,2E-02	3,4E-16
Total SUM	**1,2E+00**	**6,9E-01**	**8,6E-03**

2.3 Calibration of the 26% relative efficiency HPGe Detector

The efficiency calibration of the HPGe detector that was used for the induced activity measurements of the irradiated samples, is an important parameter that defines the feasibility of the measurement, as well as the proper planning (in terms of geometry and time) of the gamma-ray spectroscopy. The HPGe detector used was fully characterized in 2019 [34]. In order to confirm the previous characterization of the HPGe detector, a calibration point-like ^{152}Eu source was used. This source provides a variety of gamma-rays ranging, from ~100 keV up to ~1400 keV. The source was placed at several distances from the detector's window. Special care was taken on the source-to-detector-window distances that correspond to the geometry of the actual activity measurements. The intensities together with the photon energies which employed in the characterization procedure as well as a ^{152}Eu spectrum are shown in Table 2.4 and Figure 2.6, respectively.

For the determination of the efficiency curves, the absolute peak efficiency was determined using the Eq. 1.12, which can be expressed as:

$$(2.1) \qquad \varepsilon = \frac{N_{g_{counted}}}{N_{g_{emitted}}} = \frac{N_{g_{counted}}}{A \ I_g \ t_m} = \frac{N_{g_{counted}}}{A_0 \ e^{-\lambda \ \tau_{passed}} \ I_g \ t_m},$$

where $N_{g_{counted}}$ represents the net counts of the photopeak, I_g the intensity of the emitted gamma-

FIGURE 2.4. Holder dimensions.

FIGURE 2.5. Experimental set-up adopted for the irradiation.

Table 2.4: Photon energies accompanied with the intensities used for energy calibration.

Eg	244,7	344,28	367,79	411,12	443,96	778,9	867,37	964,08	1212,95	1299,1	1408
Ig (%)	7,6	26,5	0,9	2,2	3,1	12,9	4,2	14,6	1,4	1,6	21

ray, t_m the live time of the measurement, and A is the source's reference activity, λ the decay constant, and $\tau_{passesd}$ the time between the reference date and the date of the measurement.
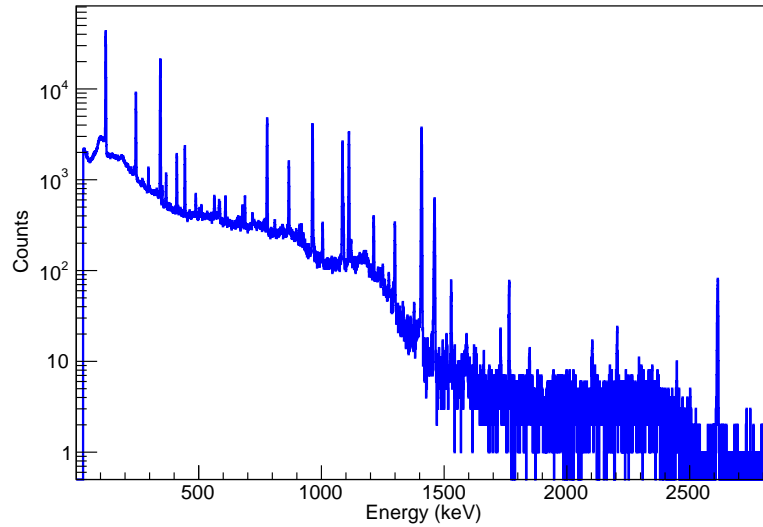
FIGURE 2.6. Spectrum of a ^{152}Eu at the source-detector distance of 9cm and for a duration of 4492 sec.

2.4 Gamma-ray measurements using the n_TOF's HPGe detector

Following the irradiation process and after a cooling time of 5 hours, required for radioprotection reasons, the foils were removed from the irradiation set-up so as for the measurement procedure to follow. This procedure was carried out using the n_TOF's 26% relative efficiency HPGe detector (CANBERRA's EGPC 25S/N 54035 p-type coaxial), cooled at 77 K [34]. Each sample' induced activity was measured off-line, one by one. A Pocket Multi-Channel Analyzer (AMP TEK Pocket MCA 8000D) was used to analyze the input signal and to store the experimental spectra of each foil.

The measurements were conducted at various source-detector distances, with the more frequent being 9 and 12 cm from the detector's window, whereas 3 cm was required for just one measurement. Several polyethylene spacers, as well as two-dimensional polyethylene rings on the center axis, were employed to accomplish the adopted distances, as well as the correct samples' position (Fig 2.7). These distances were chosen with consideration. High counting rates are always desirable so as to minimize the statistical uncertainty of the photo-peak net-area counts, which can be achieved by using close detection geometries. On the other hand, large sample-to-detector-window distances are preferred to minimize dead-time issues, pulse pile-up issues, and significant correction factors related to coincidence summing effects, sample solid angle, and geometry reproducibility. With these considerations, a specific source-to-detector-window

distance was decided in the framework of the present thesis and was realized in the activity measurements for each reaction under study.

Beside the sample-to-detector-window distance, the duration of the measurement of each sample's induced activity is also an important parameter that defines the statistical uncertainty. The measurements were performed in accordance with a plan that is provided below in Table 2.5, taking into account the half-lives of each produced isotope. Priority was given to the measurement of those radionuclides with short half-lives, followed by samples with longer half-lives or lower counting rates, which were arranged at the end of the measurement campaign. The measuring process lasted approximately three weeks. In those measurements which were feasible to be repeated, the spectra were recorded two or more times since some gamma-rays of interest might be hidden by the Compton impact of other highly active isotopes. The actual realisation of the schedule given in Appendix F. As can be seen, the measurements were ahead of schedule because the neutron flux was higher than the one obtained from the FLUKA simulations.

It has to be noted that special care and a lot of effort has been devoted to optimize the irradiation and measuring time as well as to define the characteristics of the different foils used, such as the sample's thickness and diameter. All these elements of the planning as well as the proposed source-to-detector-window distance are presented in Table 2.6.

Table 2.5: Measurement plan according to preliminary calculations.

	Sample's ID	Reaction	Actual DAQ time [h]	SD [cm]	CPS
Day 1					
10:00-11:00	W	$^{186}W(n,\ g)^{187}W$	0,030	12	9,33E+01
11:00-12:00					
12:00-17:00	Ni	$^{58}Ni(n,\ p)^{58}Co$	0,982	9	2,83E+00
		$^{58}Ni(n,\ 2n)^{57}Ni$	3,547		8,10E-01
17:00-18:00					
18:00-08:00	Al	$^{27}Al(n,\ a)^{24}Na$	5,656	9	5,58E-01
Day 2					
10:00-11:00	Cd	$^{114}Cd(n,\ g)^{115}Cd$	0,359	9	7,76E+00
11:00-12:00					
12:00-17:00	Bi	$^{209}Bi(n,\ 4n)^{206}Bi$	0,504	9	5,52E+00
		$^{209}Bi(n,\ 5n)^{205}Bi$	4,453		6,26E-01
Day 3					
10:00-14:00	Au-6	$^{197}Au(n,\ 2n)^{196}Au$	3,7902	12	7,39E-01

14:00-15:00					
15:00-03:00	Au-3	$^{197}Au(n,\ g)^{198}Au$	0,063	9	4,40E+01
		$^{197}Au(n,\ 2n)^{196}Au$	9,491		2,99E-01
Day 4					
09:00-10:00					
10:00:00	Au-1	$^{197}Au(n,\ g)^{198}Au$	0,026	12	1,09E+02
		$^{197}Au(n,\ 2n)^{196}Au$	3,286		8,52E-01
		$^{197}Au(n,\ 4n)^{194}Au$	94,524		6,15E-02
Day 7					
20:00-21:00					
21:00:00	Au-4	$^{197}Au(n,\ g)^{198}Au$	0,169	9	1,65E+01
		$^{197}Au(n,\ 2n)^{196}Au$	14,336		2,00E-01
Day 8					
12:00-13:00					
13:00-14:00	In	$^{113}In(n,\ g)^{114m}In$	0,666	9	4,17E+00
14:00-15:00					
15:00:00	Au-b	$^{197}Au(n,\ g)^{198}Au$	0,220	9	1,27E+01
		$^{197}Au(n,\ 2n)^{196}Au$	16,219		1,78E-01
Day 9					
10:00-11:00					
11:00-19:00	Sc	$^{45}Sc(n,\ g)^{46}Sc$	5,716	9	4,86E-01
19:00-20:00					
20:00:00	Au-2	$^{197}Au(n,\ g)^{198}Au$	0,092	12	3,01E+01
		$^{197}Au(n,\ 2n)^{196}Au$	5,771		4,88E-01
Day 10					
10:00:00	Co	$^{59}Co(n,2n)^{58}Co$	19,597	9	1,42E-01
		$^{59}Co(n,\ 3n)^{57}Co$	36,296		7,67E-02
Day 12					
12:00:00	Au-1	$^{197}Au(n,\ 3n)^{195}Au$	127,524	12	2,20E-02
Day 19					
17:00:00	Bi	$^{209}Bi(n,\ 3n)^{207}Bi$	163,911	9	1,70E-02
Day 29					
10:00:00					

Table 2.6: Calculations made in terms of dimensions and source-to-detector-window distances up to the selection of the optimum configuration.

Reactions	Thickness [cm]	Radius [cm]	SD [cm]	Activity (eoi) [MBq]	Activity (a1d) [MBq]
$^{114}Cd(n,\ g)^{115}Cd$	0,05	0,65	9	2,1E-02	7,6E-03
	0,05	0,15	9	1,1E-03	4,1E-04
	0,1	0,65	9	4,1E-02	1,5E-02
$^{45}Sc(n,\ g)^{46}Sc$	0,05	0,65	9	5,5E-02	5,4E-03
	0,055	0,65	9	6,1E-02	6,0E-03
	0,055	0,15	9	3,2E-03	3,2E-04
	0,03	0,15	9	1,8E-03	1,7E-04
$^{176}Lu(n,\ g)^{177}Lu$	0,05	0,65	9	6,6E-01	1,3E-01
	0,05	0,15	9	3,5E-02	7,1E-03
	0,1	0,15	9	7,0E-02	1,4E-02
$^{197}Au(n,\ g)\ \&\ (n,\ 2n)$	0,05	0,15	12	2,2E-01	1,7E-01
(n, 3n) & (n, 4n)	0,05	0,15	9	2,2E-01	1,7E-01
	0,0025	0,65	12	1,9E-01	1,4E-01
	0,0025	0,15	12	1,0E-02	7,5E-03
	0,01	0,65	12	7,5E-01	5,7E-01
	0,01	0,15	12	4,0E-02	3,0E-02
	0,01	0,15	9	4,4E-02	3,3E-02
$^{186}W(n,\ g)^{187}W$	0,05	0,65	9	4,9E-01	1,2E-01
	0,05	0,15	9	2,6E-02	6,3E-03
	0,05	0,65	12	4,9E-01	1,2E-01
$^{113}In(n,g)^{114m}In$	0,05	0,65	9	6,7E+00	2,6E-03
	0,05	0,15	9	3,6E-01	1,4E-04
$^{58}Ni(n,\ p)\ \&\ (n,\ 2n)$	0,05	0,65	9	1,7E-03	1,4E-03
$^{27}Al(n,\ a)^{24}Na$	0,05	0,65	9	1,3E-03	1,6E-04
$^{59}Co(n,\ 2n)\ \&\ (n,\ 3n)$	0,05	0,65	9	3,0E-01	2,4E-03
	0,05	0,15	9	1,6E-02	1,3E-04
$^{127}I(n,\ 2n)^{126}I$	0,05	0,65	9	1,1E-01	1,2E-03
	0,05	0,15	9	6,0E-03	6,7E-05
$^{209}Bi(n,\ g)\ \&\ (n,\ 3n)$	0,1	0,65	9	1,5E-02	5,0E-03
(n, 4n) & (n, 5n)	0,1	0,15	9	7,8E-04	2,6E-04
$^{139}La(n,\ g)^{140}La$	0,05	0,65	9	1,8E-02	1,2E-02
	0,05	0,15	9	9,4E-04	6,2E-04
$^{54}Fe(n,\ p)\ \&\ (n,\ a)$	0,05	0,65	6	5,7E-04	5,7E-04
	0,05	0,15	6	3,0E-05	3,0E-05

FIGURE 2.7. The HPGe detector at n_TOF/CERN along with polyethylene spacers and rings.

2.5 Neutron flux

The irradiation was performed between September and October 2021 at the newly built experimental area, the NEAR station of the n_TOF facility at CERN.
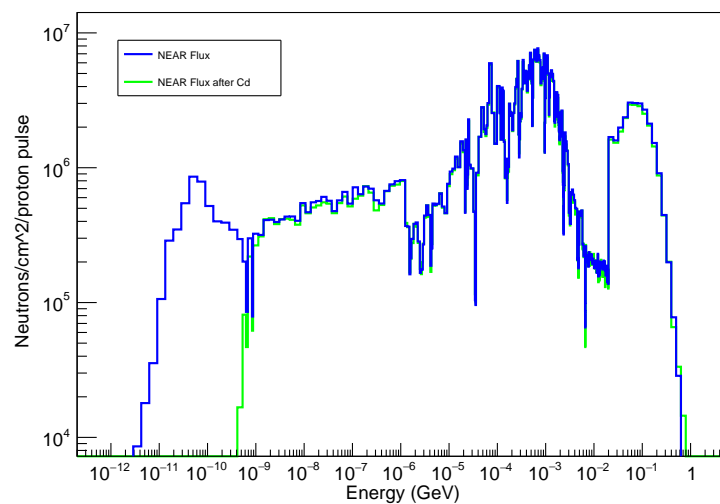
FIGURE 2.8. The FLUKA-simulated neutron flux at NEAR Station (blue), and its absorption by a cadmium foil of 1mm thickness using the MCNP 5 Monte-Carlo simulation code (courtesy of S. Chasapoglou).

For almost three weeks, from 28/09 at 09:55 to 20/10 at 05:08, the chosen foils were irradiated at the center of the beam, utilizing approximately 1.9E+18 protons. For the graphical representation of the NEAR's beam flux via ROOT, the *isolethargic binning* was adopted, which, in principle, is a fixed binning width on the logarithm instead of linear, e.g. $log(x_{i+1}) - log(x_i) = const$ (Fig. 2.8).

DATA ANALYSIS & GEANT4 SIMULATIONS

T he analysis procedure's aim is to analyze the experimental spectra in order to extract a precise estimation of the induced activity of each reference reaction. The findings, coupled with the initial "guess" spectrum, will be used as an input for an unfolding algorithm towards to the estimation of the neutron beam energy distribution. Nevertheless, the unfolding procedure is not in the scope of the present work.

3.1 Data Analysis

The analysis of the acquired pulse height spectra from Monte-Carlo simulations as well as from the actual activity measurements was done through a ROOT-based code in conjunction with the TV gamma-spectroscopy software. The basic concept among these gamma-ray analysis methods is that a Gaussian fit is applied at the photopeaks of interest in order to estimate the counts, followed by a polynomial fit to subtract the background. In other words, the net counts N are given from the gross counts N_s in the peak area subtracted by the background counts N_b. The uncertainty which corresponds to net counts is given by $\sqrt{N_s + N_b}$ [28]. The first experimental spectrum of each sample is depicted below (see Fig.3.3), along with a background spectrum at the same Data Acquisition time (DAQ time).

The spectra were saved regularly during the measurements to ensure the proper data collection and to validate that the peak growth rate is compatible with the decay constant of the isotope under study. This allows for the identification of possible contamination issues as well as the simpler solution of gain-shift problems.
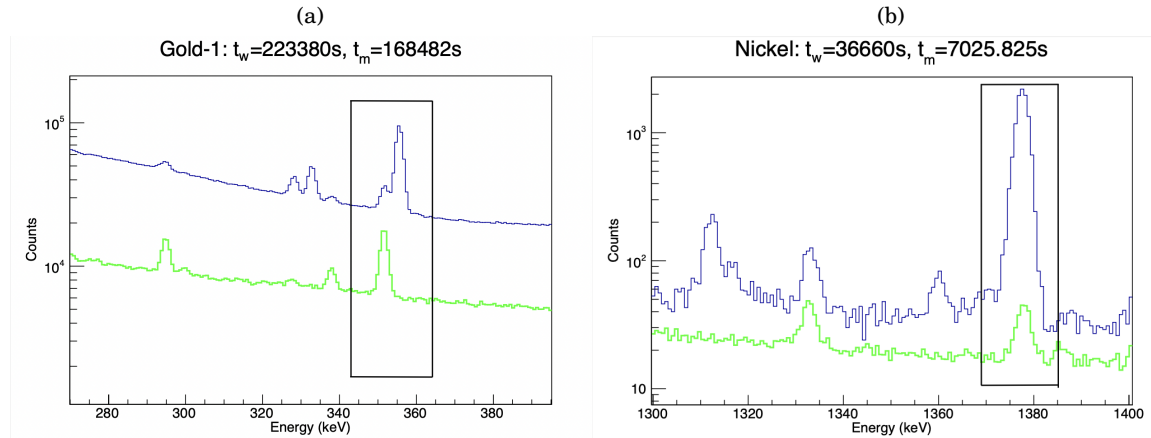
FIGURE 3.1. Contaminant peak in (a) Gold-1 355keV, and (b) Nickel 1377keV physics cases.

With the aforementioned operations accomplished, the following analysis phase is the activity's determination of secondary peaks of each process. During this phase, all the gamma-rays could be utilized to evaluate the sample's activity in order to investigate if the photopeaks of interest have an external contribution, either from background activity or another isotope. Upon this, a comparison in activity between the secondary peaks and the photopeaks of interest that had already been analyzed was performed.

As the above Figure 3.1 shows, some peaks of interest were contaminated by the background radiation. In these cases, background subtracted spectra were used. For that purpose a very long background measurement was taken with the identical settings in the pulse shaping electronics. The background spectrum's excellent statistical uncertainty was instrumental for those physics cases when the background subtraction method had to be applied.

3.2 GEANT4 Monte-Carlo Simulations

To determine the needed correction factors for the detection efficiency that are related to the extended geometry of the sample and the self-attenuation of the gamma-rays within the sample material, Monte-Carlo (MC) simulations using the GEANT4 toolkit were performed. The GEANT4 MC simulations were bench-marked by considering the point source geometry adopted during the experimental efficiency calibration measurements. Inconsistencies of less than 5% were discovered between experimental efficiency data and the GEANT4 simulations. When dealing with low-energy gamma-ray energies ($E_g < 100$ keV: ^{59}Co (n, 3n) ^{57}Co, ^{197}Au (n, 3n) ^{195}Au) the detection efficiency has to be determined exclusively by GEANT4 simulations. This is due to

the fact that in this energy range, the Al-window of the detector causes significant attenuation of the low energy photons, making the extrapolation of the fitting efficiency curves inadequate. Furthermore, the GEANT4 simulations allow the inclusion of the isotope's under study full decay scheme. As a result, the effect of coincidence summing effects was also considered in the analysis procedure [28]. This effect is important when short sample-to-detector-window distances are adopted (3 cm). The detector efficiency at each distance is shown in Table 3.1 for the various gamma-ray energies emitted when:

1. a point source with the decay schemes are adopted,

2. extended sources are adopted but not the decay schemes, and

3. extended sources along with the decay schemes are adopted.
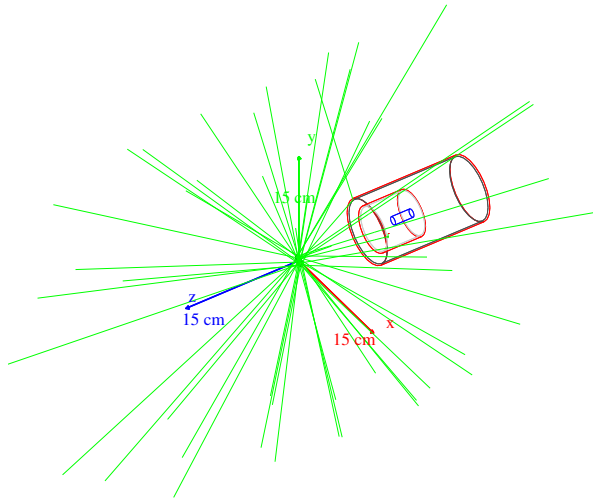
FIGURE 3.2. Visualization of the simulation of an extended source via GEANT4 toolkit.
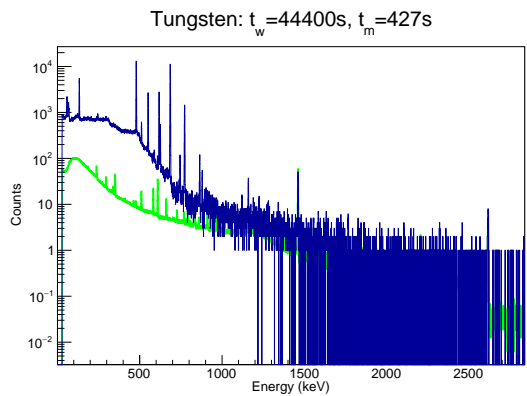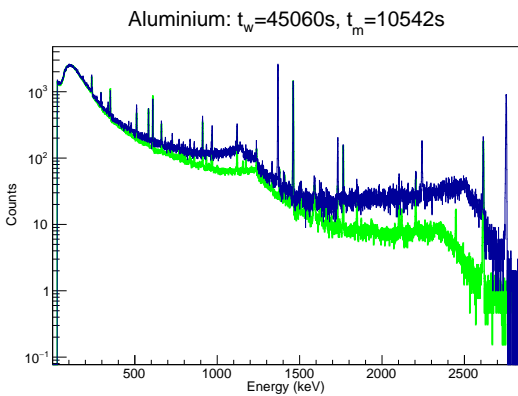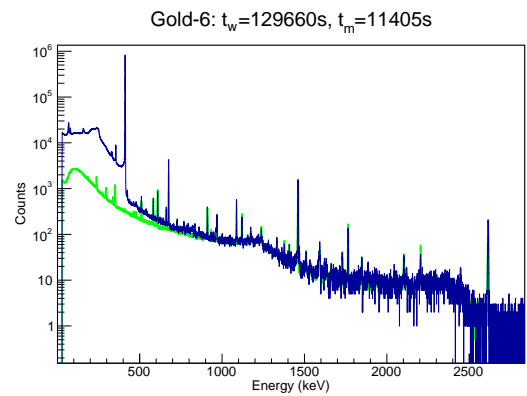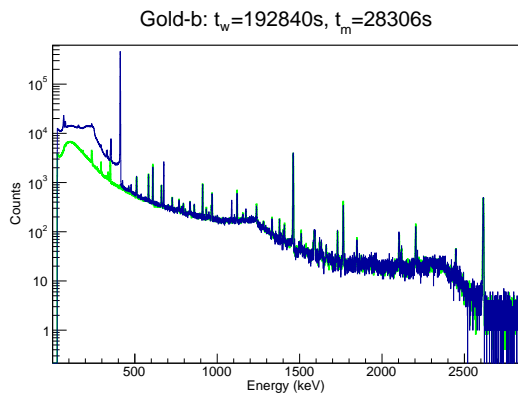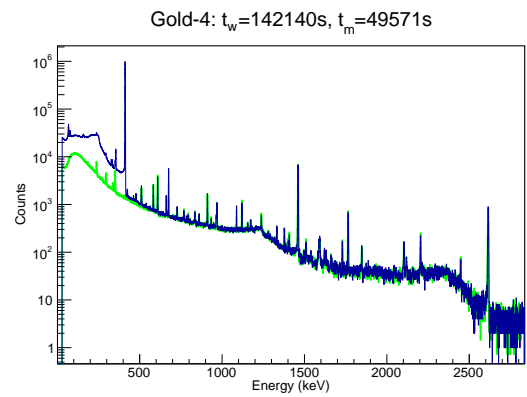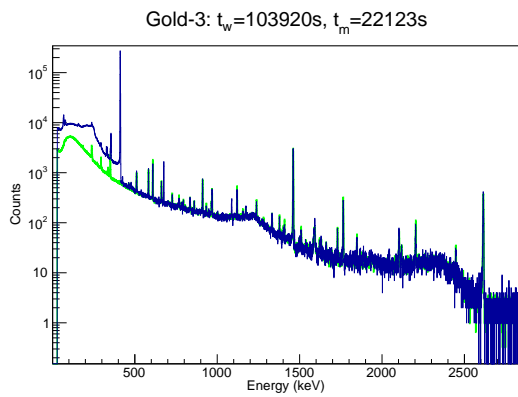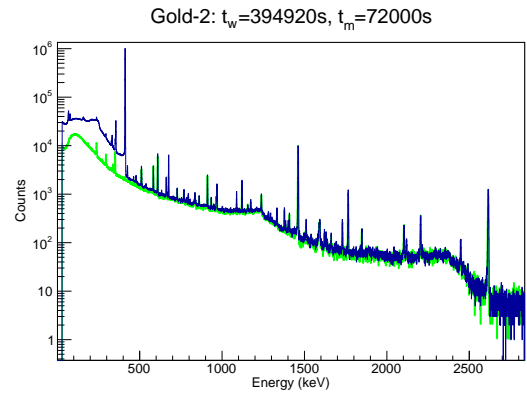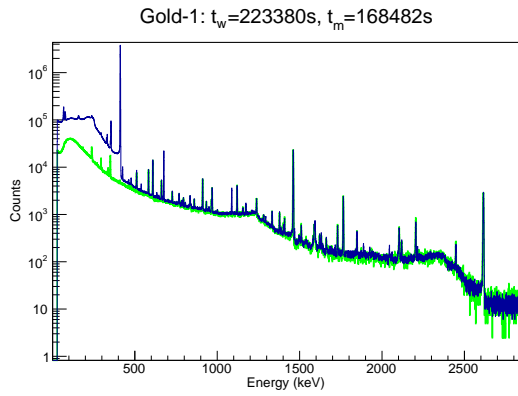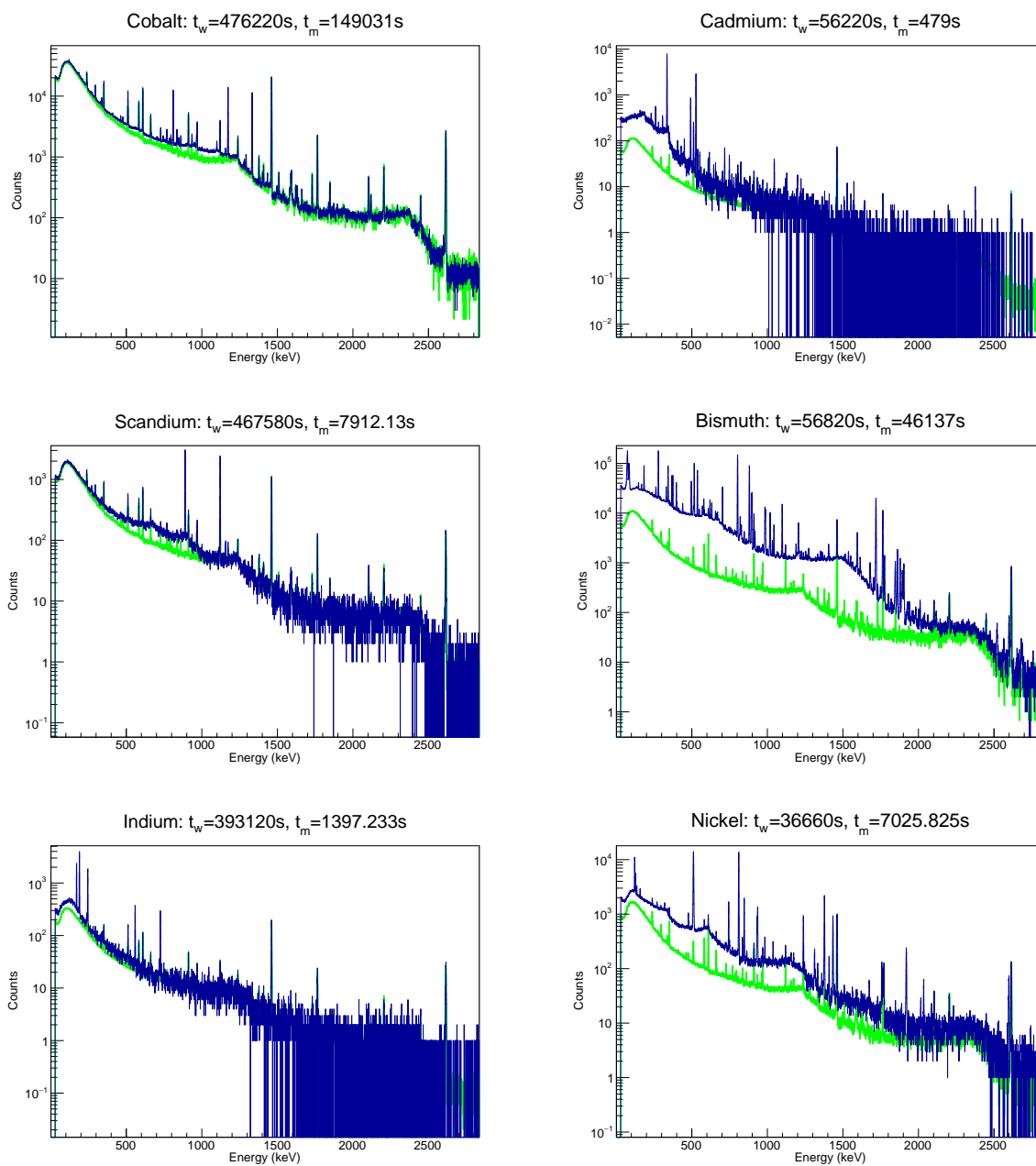
FIGURE 3.3. The first experimental spectrum of each foil accompanied with a background spectrum (green line) with the same DAQ time.

Table 3.1: Efficiencies from GEANT4 toolkit.

Sample ID	Thickness [mm]	Diameter [mm]	Eff at SD [cm]	Reaction	Eff of PS	Eff of Iso	Eff of G-rays
Au1	0.5	3	12	**197Au (n, g) 198Au**	0,003086394	0,002807362	0,00284018
				197Au (n, 2n) 196Au	0,003497667	0,00311746	0,00313788
				197Au (n, 4n) 194Au	0,00365828	0,00330121	0,00330456
Au3	0.1	3	9	**197Au (n, g) 198Au**	0,00483517	0,004767298	0,00481782
				197Au (n, 2n) 196Au	0,005500161	0,005428552	0,00544089
Au-6	0.025	13	12	**197Au (n, 2n) 196Au**	0,003489483	0,00344245	0,00353629
In	0,5	13	9	**113In (n, g) 114In m**	0,0097991	0,00919505	0,0087076
Sc	0.3	3	9	**45Sc (n, g) 46Sc**	0,002040735	0,00204035	0,00207626
W-3	0.5	13	12	**186W (n, g) 187W**	0,001920157	0,00185359	0,00191523
Bi	1	13	9	**209Bi (n,3n) 207Bi**	0,002122	0,00206828	0,0020972
				209Bi (n, 4n) 206Bi	0,002604485	0,00260448	0,00262311
				209Bi (n, 5n) 205Bi	0,001381963	0,00130538	0,00137961
Cd	1	12,7	9	**114Cd (n, g) 115Cd**	0,003899199	0,00369592	0,00371497
Co	0.5	3	9	**59Co (n, g) 60Co**	0,001778409	0,00177432	0,00177191
				59Co (n, 2n) 58Co	0,002687149	0,00261606	0,00266487
				59Co (n, 3n) 57Co	0,009985666	0,00951349	0,00955012

Al	0,47	13	9	**27Al (n, a) 24Na**	0,001747022	0,00169305	0,00173146
Ni	0.5	13	9	**58Ni (n, p) 58Co**	0,002788627	0,00272798	0,00264786
				58Ni (n, 2n) 57Ni	0,001713709	0,00167960	0,00170765

Along with the aforementioned measurements, a background spectrum was obtained to affirm that no background peaks coincided with the photopeaks of interest (see Fig. 3.4). All these measurements were performed at CERN's n_TOF Electronics Lab.
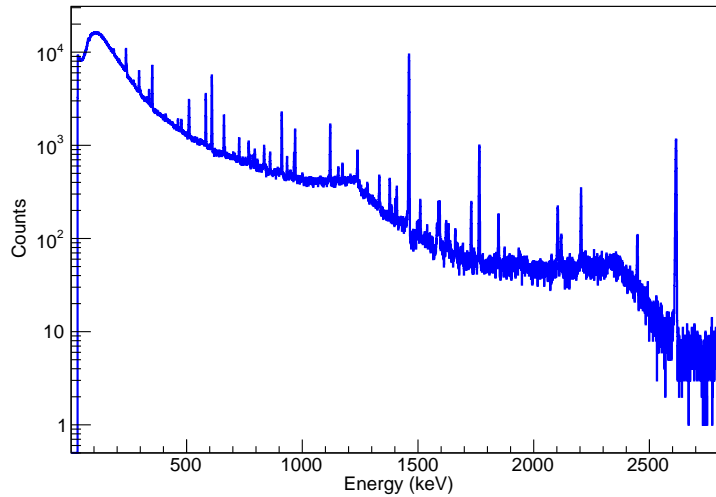
FIGURE 3.4. A background spectrum recorded at n_TOF's Electronics Lab over a period of 68359 sec.

3.3 f_b correction factors

3.3.1 Conditions of the proton beam

During the irradiation, the neutron flux did not remain constant. Consequently, a method of monitoring these fluctuations is essential, as they may have an adverse affect on the activation operation, particularly in those radio-nuclides with a short half-life (Al, W, Cd, etc.). For this purpose, the accurate proton beam conditions were recorded through the CERN's TIMBER database. Using a multi-channel scaler (MCS), one was able to extract a file with the total protons per seconds over time, as seen in Figure 3.5, resulting in a summing flux file. A much more detailed report is presented in Appendix B. Afterward, this file was used as an input in a ROOT-based script to calculate the correction factors in order to compare the feasibility and the experimental results (see App. C).

In the calculations for the expected counting rates and the scheduling of the measurement campaign the decay during irradiation has been taken into account assuming constant neutron flux. In order to properly compare the calculated and corresponding experimental activities, the fluctuations of the neutron beam have to be considered. The following Table 3.2 provides

information on the execution and sequence of measurements that finally took place.
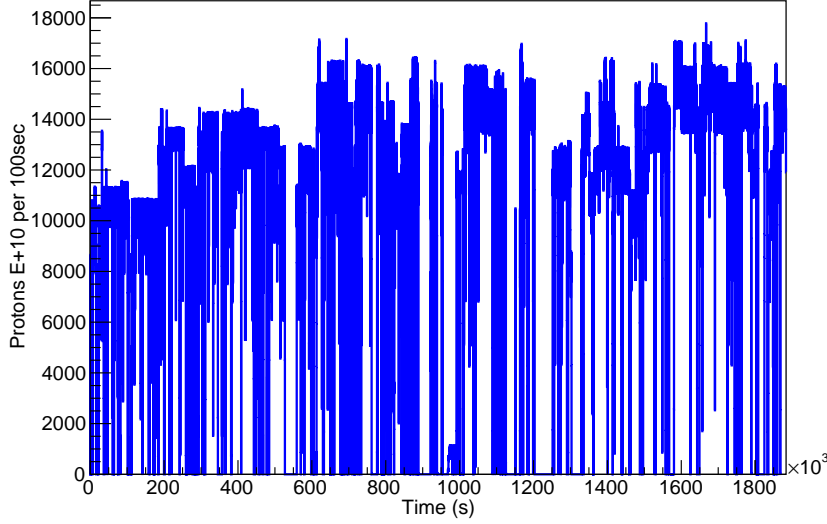
FIGURE 3.5. Proton beam fluctuations during the irradiation.

Experimental Activities

The experimental determination of each foil's activity was determined by means of the following equation:

$$(3.1) \qquad A = \frac{Counts\,(\frac{1}{f_b})\,(1 - e^{-\lambda t_{irr}})}{\varepsilon\,I_g\,e^{-\lambda t_w}\,(1 - e^{-\lambda t_m})\,t_{irr}}$$

where again Counts represent the recorded counts in the photopeak of interest, $\frac{1}{f_b}$ the total correction factor that corresponds to the decay during the irradiation including the actual fluctuations of the neutron flux as taken from the CERN's TIMBER data-base, I_g is the intensity of the emitted gamma-ray, ε the detector's efficiency for the emitted gamma-ray taken from GEANT4 simulation (3rd option), λ the decay constant of the product nucleus, t_m the measuring time of the induced activity, t_w the waiting time between the end of the irradiation and the start of measurement, and t_{irr} the time duration of the irradiation's procedure.

The intensities for the gamma-ray lines used in the analysis are given in Table 2.1, Table 3.2, and the total f_b factor as listed in Table 3.3 below. Moreover, in the Table 3.3, there is also a column for these physics cases the background subtracted spectrum was used for the

43

Table 3.2: The actual starting and stopping time of the activity measurements for each reaction. In the fourth column, the activity for constant neutron flux is given. The f_b factor is the correction for the neutron beam fluctuations, and the product is the theoretical activity estimation corrected for the actual fluctuations of the neutron flux.

Sample	Reaction	Start	End	A [Bq]	fb	A*fb
Ni	(n, p)	20/10/21 15:19	20/10/21 17:17	1,088E+03	0,995648	1,083E+03
	(n, 2n)			3,833E+02	0,840858	3,223E+02
W	(n, g)	20/10/21 17:28	20/10/21 17:34	1,896E+05	0,838338	1,589E+05
Al	(n, a)	20/10/21 17:39	20/10/21 20:35	3,925E+02	0,848727	3,331E+02
Cd	(n, g)	20/10/21 20:45	20/10/21 20:53	1,171E+04	0,861596	1,009E+04
Bi	(n, 3n)	20/10/21 20:55	21/10/21 09:46	4,736E+00	0,999974	4,736E+00
	(n, 4n)			2,481E+03	0,941528	2,336E+03
	(n, 5n)			1,499E+03	0,978006	1,466E+03
Au3	(n, g)	21/10/21 10:00	21/10/21 16:10	1,971E+04	0,876134	1,7269E+04
	(n, 2n)			8,492E+01	0,940931	7,9904E+01
Au6	(n, 2n)	21/10/21 17:09	21/10/21 20:20	3,291E+02	0,940931	3,0966E+02
Au4	(n, g)	21/10/21 20:37	22/10/21 10:26	2,068E+04	0,876134	1,8118E+04
	(n, 2n)			8,911E+01	0,940931	8,3846E+01
Aub	(n, g)	22/10/21 10:42	22/10/21 18:36	2,054E+04	0,876134	1,7996E+04
	(n, 2n)			8,851E+01	0,940931	8,3282E+01
Au1	(n, g)	22/10/21 19:11	24/10/21 18:10	9,840E+04	0,876134	8,621E+04
	(n, 2n)			4,240E+02	0,940931	3,990E+02
	(n, 4n)			1,473E+02	0,843006	1,242E+02
In	(n, g)	24/10/21 18:20	24/10/21 18:43	3,079E+03	0,993696	3,060E+03
Au2	(n, g)	24/10/21 18:50	25/10/21 14:53	9,882E+04	0,876134	8,658E+04
	(n, 2n)			4,258E+02	0,940931	4,006E+02
	(n, 4n)			1,480E+02	0,843006	1,248E+02
Sc	(n, g)	25/10/21 15:01	25/10/21 17:13	2,559E+02	0,996336	2,550E+02
Co	(n, g)	25/10/21 17:25	27/10/21 10:53	1,171E+02	0,999844	1,171E+02
	(n, 2n)			5,829E+01	0,995648	5,804E+01
	(n, 3n)			6,641E+00	0,998890	6,634E+00

determination of the photo-peak net area counts. The results of the determined activity are given in the same table.

Table 3.3: Information needed for the induced activities determination, the correction factor f_b, and the activity expressed in Becquerel.

Sample ID	Reaction	Contamination	1/fb	A [Bq]
Cd	114Cd(n, g)115Cd	none	5,85134	2.295E+04
Sc	45Sc(n, g)46Sc	$\checkmark$	1,08887	6.480E+02
Au-1	197Au(n, g)198Au	none	4,93015	6.664E+04
	197Au(n, 2n)196Au	none	2,51815	7.700E+02
	197Au (n,3n) 193Au			
	197Au(n, 4n)194Au	$\checkmark$	8,0053	4.270E+02
Au-2	197Au(n, g)198Au	none	4,93015	6.135E+04
	197Au(n, 2n)196Au	none	2,51815	7.484E+02
	197Au(n, 4n)194Au	$\checkmark$	4,93015	4.110E+02
Au-6	197Au(n, 2n)196Au	none	2,51815	5.933E+02
Au-3	197Au(n, g)198Au	none	4,93015	1.196E+04
	197Au(n, 2n)196Au	none	2,51815	1.522E+02
Au-4	197Au(n, g)198Au	none	4,93015	2.260E+04
	197Au(n, 2n)196Au	none	2,51815	1.578E+02
Au-b	197Au(n, g)198Au	none	4,93015	2.091E+04
	197Au(n, 2n)196Au	none	2,51815	1.574E+02
W	186W(n, g)187W	none	12,8172	1.985E+05
In	113In(n, g)114In m	none	1,15303	6.622E+03
Ni	58Ni (n, p) 58Co	none	1,10558	2.882E+03
	58Ni(n, 2n)57Ni	$\checkmark$	8,56599	1.092E+03
Al	27Al(n, a)24Na	none	20,5757	1.111E+03
Co	59Co(n, g)60Co	$\checkmark$	1,00377	1.882E+02
	59Co(n, 2n)58Co	none	1,10558	1.2227E+02
	59Co(n, 3n)57Co	none	1,02691	1.279E+01
Bi	209Bi (n,3n) 207Bi	none	1,00063	1.632E+01
	209Bi(n, 4n)206Bi	$\checkmark$	2,50118	5.198E+03
	209Bi(n, 5n)205Bi	$\checkmark$	1,53876	2.460E+03

PRELIMINARY RESULTS

The final activities have been corrected for the contamination caused by the background spectrum and have been verified using the most intense gamma-ray of the spectra in different occasions (waiting and measuring time), as well as by additional gamma-rays from the same decay line.

The ratio of experimental activity to estimated activity in connection with each reaction is depicted in Figures 4.1 - 4.4 below. It can be observed in the low neutron energy area in the first graph, which is represented by the capture reactions. Five of the six reactions were placed in the upstream holder so that they could be directly compared to the findings. The reaction for which the sample was placed in the downstream holder corresponds to the ^{59}Co (n, g) ^{60}Co, and is indicated in the results. However, the beam that passed through the Au-1 foil was attenuated due to the presence of another sample in front, and a correction should be made in this case. This correction necessitates more analysis using the GEANT4 toolkit package, which will take a long time and is outside the project's scope. As it concerns the (n, g) reaction of the gold foils, Au-1 and Au-2, the findings are compatible with each other.

The threshold reactions are depicted in the next figures (4.2 - 4.4). The reactions that were placed in the upstream holder appear to be a factor of two with three, resulting in the actual flux in that area being greater than the FLUKA-simulated neutron flux. However, the downstream holder reactions should again be modified by a correction factor such that the feasibility values are directly equivalent to the experimental values. Again, the reaction (n, 2n) of all the gold foils, Au-1, Au-2, Au-3, Au-4, Au-b, and Au-6, the results are also consistent. These gold foils were placed in the upstream and downstream holders, confirming what has already been said at the

outset, that threshold reactions remain unaffected by the presence of another foil in front of them. The same compatible results apply to the (n, 4n) reaction of the Au-1 and Au-2 foils.

After this initial step of the NEAR beam characterization, the FLUKA-simulated neutron flux seemed to have been underestimated in comparison with the calculated results. Nevertheless, the inclusion of more correction factors has to be taken into account in order to properly compare with the FLUKA simulations.

Furthermore, the FLUKA simulations are being revisited at the moment so the new simulated flux might agree better with the experimental results occurred from this work.
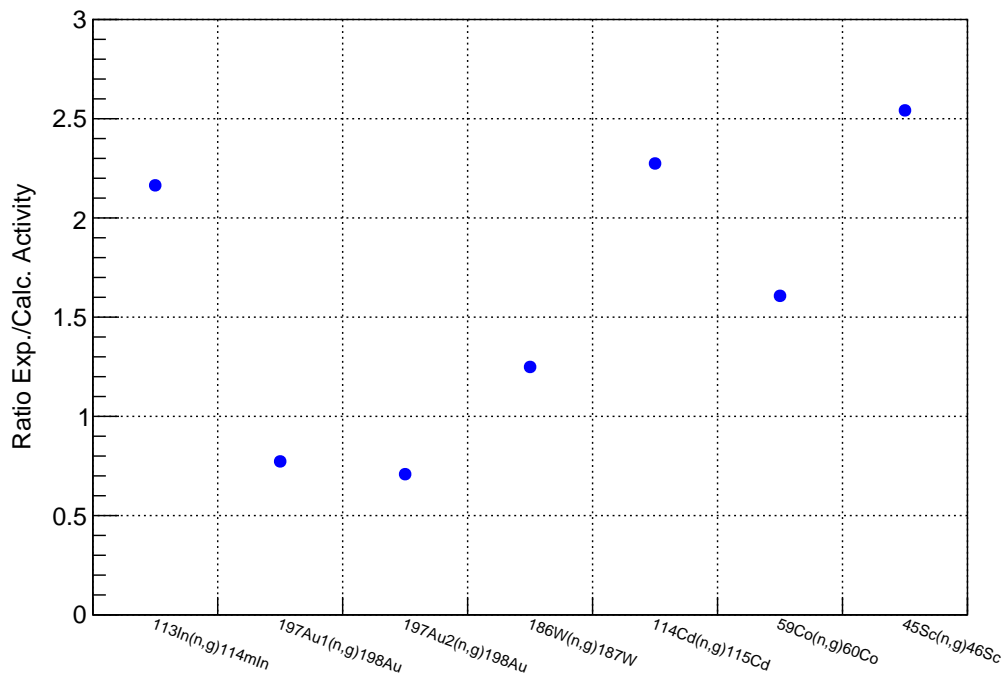
FIGURE 4.1. Preliminary results for capture reactions.
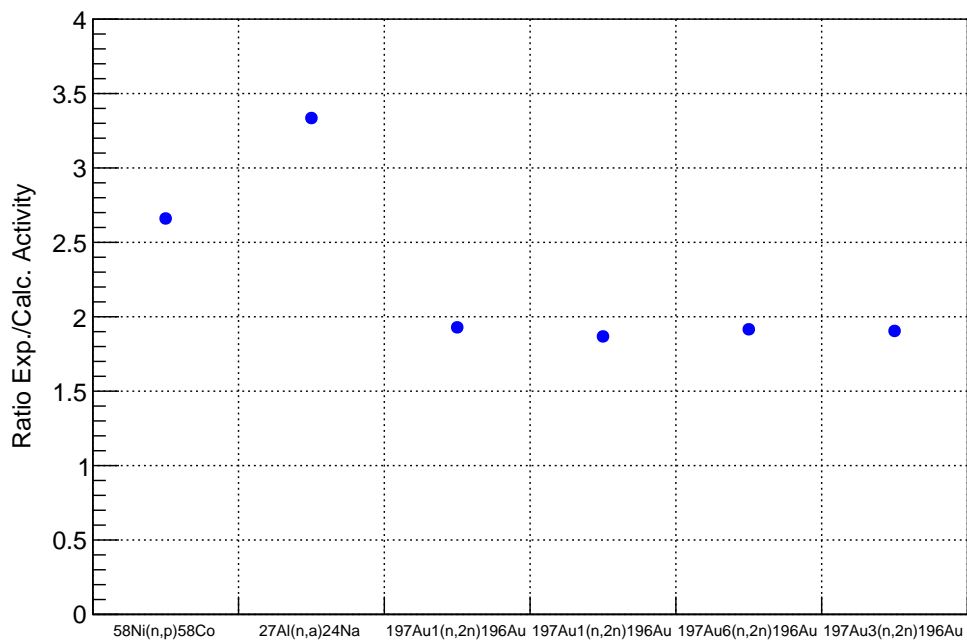
FIGURE 4.2. Preliminary results for threshold reactions.
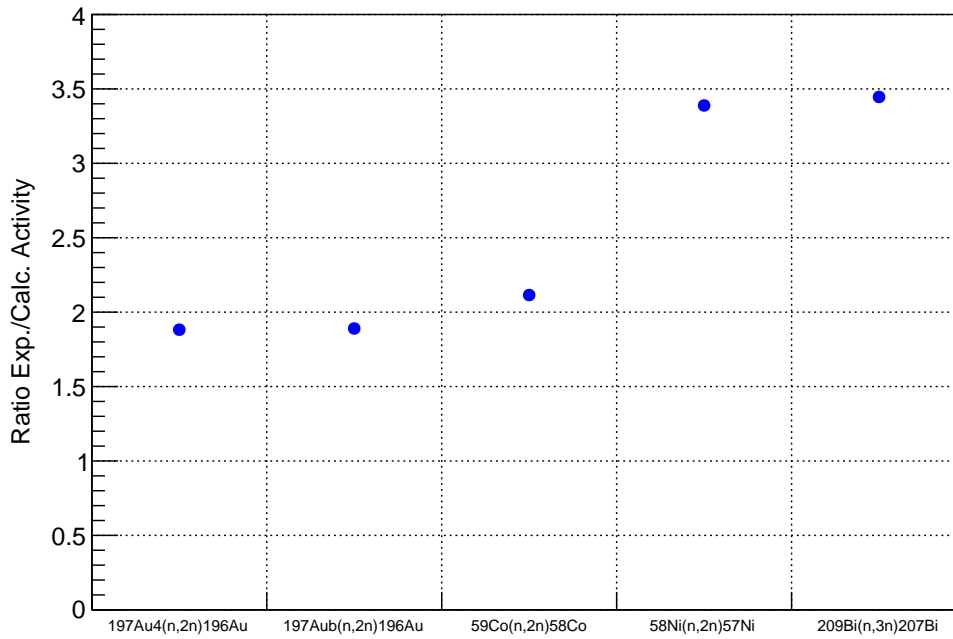
FIGURE 4.3. Preliminary results for threshold reactions.
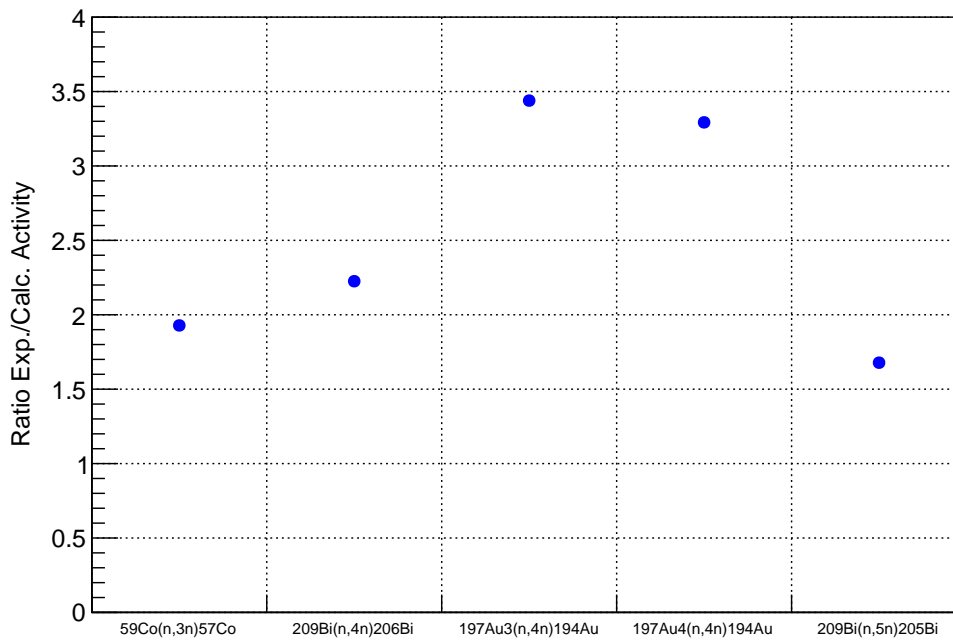
FIGURE 4.4. Preliminary results for threshold reactions.

CONCLUSION AND PROSPECTIVE

5.1 Conclusions

The NEAR Station experimental area was constructed during the LS2 of CERN. As the experimental area is novel at n_TOF, a multi-foil activation campaign was adopted for the characterization of the neutron beam. Nevertheless, the characterization is challenging on the grounds that the flux covers approximately eleven orders of magnitude in energy. In this work, the planning of this first multi-foil activation study was realized. Furthermore, the first experimental results are discussed, and a preliminary comparison with expected rates is presented. Various materials in the form of foil were irradiated for almost 22 days, followed by gamma spectroscopy measurements. The induced activities of the 17 reactions under investigation were performed using the 26% relative efficiency HPGe Detector. The samples were placed one by one in front of the HPGe according to the measurement plan. As an outcome, from the comparison of experimental with calculated activities, the simulated flux seems to have been underestimated.

5.2 Perspectives

For future analysis, a much more detailed study is required, i.e., the correction factor for neutron self-shielding within each sample has to be considered. The induced saturated activities from the present work are already presented and shared within the n_TOF collaboration. These activities are going to be used in neutron spectrum unfolding codes (INFN - Bari n_TOF group, University of Granada group, NTUA group). Following the characterization of the NEAR neutron beam, the possibility of shaping the neutron energy distribution to Maxwellian-Spectra corresponding to various stellar temperatures will be investigated. This can be done

using different B_4C and aluminum filters. For this study, an approved proposal from the CERN INTC committee is already under development.

A

The production rate is given by the following formula:

$$(A.1) \qquad \frac{dN}{dt} = \sigma\, f(t)\, N_T - \lambda\, N$$

The integral of this differential equation results in the next formula:

$$N(t) = \frac{\int e^{\int \lambda\, dt} \sigma\, f(t)\, N_T + C}{e^{\int \lambda\, dt}}$$

$$N(t) = \int_0^{t_{irr}} f(t)dt\; \sigma\, N_T\; \frac{\int_0^{t_{irr}} e^{\lambda t}\, f(t)}{\int_0^{t_{irr}}\, f(t)} e^{-\lambda t_{irr}}$$

$$N(t) = \sigma\, N_T\, \Phi\, \frac{1 - e^{\lambda t_{irr}}}{\lambda t_{irr}}$$

$$(A.2) \qquad N(t) = \sigma\, N_T\, \Phi\, f_b$$

The counts per second recorded by the HPGe detector could be calculated as following:

$$cps = \varepsilon\, I\, \frac{dN}{dt}$$

$$cps = \varepsilon\, I\, \lambda\, N$$

$$cps = \varepsilon\, I\, \lambda\, N_0\, e^{-\lambda t}$$

53

Integrating this formula for the time interval from t_m to $t_m + t_w$:

$$counts = \varepsilon\ I\ \lambda\ N_0 \int_{t_m}^{t_m+t_w} e^{-\lambda t_m}\ dt$$

(A.3)
$$counts = \varepsilon\ I\ N_0\ e^{-\lambda t_w}(1 - e^{-\lambda t_m})$$

The eq. A.3 gives the number of counts acquired at the end of the measurement. In conjunction with the eq. A.2, the equation of the cross-section used in activation technique can be obtained:

$$\sigma = \frac{counts\ CF}{N_T\ \Phi\ \varepsilon\ I_\gamma\ (1 - e^{-\lambda t_m})\ e^{-\lambda t_w}\ f_b}.$$

B

ROOT SCRIPT FOR SUMMING FLUX

R oot-based code builded up in the C++ language, for the processing of the TIMBER data as to be used for the correction for the beam's fluctuations.

```cpp
#include <iostream>
#include <fstream>
#include "TH1.h"
#include "TCanvas.h"
#include "TGraph.h"
#include "TFile.h"
#include "TStyle.h"
#include "Riostream.h"
#include "TMath.h"
#include "TLegend.h"

using namespace std;


void mcs()
{
  gROOT->Reset();
  gStyle->SetOptStat(0);

  system("./timb");


TCanvas *c1 = new TCanvas ("c1","NEAR Station at n_TOF",700,500);


  //---------------Open TIMBER file--------------------//

  ifstream timber;
  timber.open("TIMBER_data_28_09_20_10.txt");

  //int max_lines=225477; //terminal: wc -l
  int max_value=1.88355e+06;
  double intensity[248007]={0.};
  double time[248007]={0.};


  //---------------Create the histogram------------------//


  TH1D* histo_sum = new TH1D("histo_sum", "", max_value/100, 0.0, max_value);


  //----------------------------------------------------//


  int i=0;
  double sum_int=0.;
  while (!timber.eof())
    {
      timber >> time[i] >> intensity[i];
      sum_int+=intensity[i];

      for (int k=0;k<intensity[i];k++){
          histo_sum->Fill(time[i]);
      }
      i++;
```

```
    }
timber.close();

  //--------------------------------------//

  cout<<endl<<"***************************************************"<< endl << endl;
  cout << "Number of protons from 28/09 09:55 till 20/10 05:08 : " << sum_int*(1e10) << endl << endl;
  cout << "Number of protons per week : " << sum_int*(1e10)/3 << endl<< endl;
  cout << "Number of protons per day : " << sum_int*(1e10)/21 << endl;
  cout<<endl<<"***************************************************"<< endl << endl;


  //-------------------------------------//


  histo_sum->SetLineColor(4); //blue
  histo_sum->SetLineWidth(2);

  histo_sum->GetXaxis()->SetTitle("Time (s)");
  histo_sum->GetXaxis()->CenterTitle();
  histo_sum->GetYaxis()->SetTitle("Protons E+10 per 100sec");
  histo_sum->GetYaxis()->CenterTitle();

histo_sum->Draw("histo");


  //-------------------------------------//


  c1->Modified();
  c1->Update();
  c1->SaveAs("#Protons per 100s.pdf");


  //-----------------------------------------------//


  TFile *TIMBER = new TFile("TIMBER_NEAR.root", "RECREATE");
  histo_sum->Write();
  TIMBER->Close();

  //-----------------------------------------------//

  Double_t a,b,c;
  Int_t n = histo_sum->GetNbinsX();
  ofstream outfile("Summing_Flux_NEAR.dat");
  for (Int_t i=1; i<=n; i++) {
     a=histo_sum->GetBinLowEdge(i) + histo_sum->GetBinWidth(i);
     b=histo_sum->GetBinContent(i);

  outfile << a << "\t" <<  b << endl;
    }


  //------------------Legend for canvas-----------------//
```

ROOT-BASED CODE FOR THE f_b CORRECTION FACTOR

D etermination of f_b correction factor. The user should provide information such as the half-life of the produced radionuclied in seconds, the flux file, the number of channels till the irradiation, and the overall time of each channel expressed in seconds. The correction for feasibility calculations that have already been corrected by the ROOT-code for the decay during irradiation, should multiply the results by the factor $Partial\_correction$. The correction that corresponds to the experimental results also includes the correction for the non-constant beam, but also the decay during the irradiation and for this, the results will be multiplied by the factor $Total\_correction$.

```cpp
# include <iostream>
# include <math.h>
# include <fstream>
# include <stdlib.h>


using namespace std;
int FluxCorrections() {


  char file[20];
  int channels;
  double chan;
  double flux[30000];
  double time_duration;
  double t_irr;
  double sum1=0., sum2=0.;
  double Total_correction;
  double Partial_correction;
  double lamda ,halfLife;

  cout<<"Give the lalf life of the reaction product in seconds: ";
  cin >>halfLife;

  lamda = log(2)/halfLife;

  cout <<"give the name of the flux monitor file (two columns: channel intensity):  ";
  cin >>file;

  cout <<"give the number of channels until the end of irradiation:  ";
  cin >>channels;

  cout <<"give the time duration of each channel in sec:  ";
  cin >> time_duration;




  ifstream in;
  in.open(filen);
  for (int i=0;i<channels;i++)
    {
     in >>chan;
     in >>flux[i];
    }

  T_irr=channels* time_duration;

  cout << "The total time of irradiation was :  "<< t_irr <<"  sec"<<endl;

  for (int k=0;k<channels;k++)
    {
     sum1=flux[k]+sum1;
     sum2=sum2+flux[k]*(exp((k+1)*lamda*dt)-exp(k*lamda*time_duration));
    }
```

```cpp
Partial_correction =sum1*(exp(lamda*tact)-1)/(sum2*numChan); //corection factor for the already corected

Total_correction=sum1*lamda*dt/(sum2*exp((-lamda)*tact));

cout <<"For the cross section value corrected already for the decay during activation\n";
cout <<"The corection for the non constant neutron flux during activation is: ";
cout <<endl<< Partial_correction <<endl;


cout <<"The overall correction factor including the decay during activation and flux fluctuations is
        (1/fb):"<<endl;

cout <<endl<<Total_correction<<endl;

return 0;
}
```

ROOT-BASED CODE FOR EXPECTED COUNTING RATE ESTIMATIONS USING THE ACTIVATION TECHNIQUE

Root-based code utilized for expected activity and counting rate estimation. The user must provide a set of files with the required information. The user should provide the simulated neutron flux file, the cross-section file of the reaction under study, a file of irradiation and measurement conditions, and a file with information about the sample.

Simulated flux file

First there should be provided the simulated flux file which consists of 4 columns, the lower and upper edge of the bin, the bin content (the neutrons), as well as one more column which is represented the bin content error.

Cross Section file

The file of the cross-section consists of two columns, the first one of which gives the neutron energy expressed in eV and the other gives the value of the cross-section in barn.

Irradiation file

This file provides information such as the number of protons used during the irradiation, the irradiation time as well as the waiting and measuring time expressed in hours.

Sample file

which includes the mass in grammar, the abundance of the stable isotope, the mass number and the atomic mass, the element symbol, the produced radionuclide's half-life expressed in hours,

the intensity of the emitted gamma-ray with a maximum value of one, the absolute detector's
efficiency ($0<\varepsilon<1$), and, finally, the radius of the sample in centimeter.

The code [1] is given within the next pages .

---

[1]Basic Author: Elisso Stamati, Developer: Styliani Goula

```cpp
//=============================================================================//
//                    Expected Counts For NEAR activation                      //
//=============================================================================//

// Headers
#include <iostream>
#include <fstream>
#include <vector>
#include <cstdio>
#include <math.h>
#include <sstream>
#include <fstream>
#include "TH1.h"
#include "TGraph.h"
#include "TCanvas.h"
#include "TFile.h"
#include "TRandom3.h"
#include "TSystem.h"
#include "TStyle.h"

using namespace std;

//====================================
// Global Variables

string FLUX_FILE="input_flux.dat"; //Name of the flux file

const int BINS = 269; // Number of bins (lines wc-l) in flux file
double EDGES[BINS+1]; // Bin edges for the flux histogram (turned into eV)
double NEUTRONS_TOTAL[BINS]; // Total number of neutrons in each energy bin /cm2
double NEUTRONS_FOR_SACS[BINS]; // Enough statistcs to loop each bin to calculate SACS

const double PI = 3.14159;
const double AVOGADRO= 6.022e23;

double LAST_XS_ENERGY; // The last energy for which the xs is given
double FIRST_XS_ENERGY; // The first energy for which the xs is given

TGraph *XS_Graph = new TGraph(); // Cross section grap
TH1F *Flux_Histo = new TH1F(); // Flux histogram
TH1F *Sampling_Histo = new TH1F(); // Flux histogram used for sampling -> SACS calculation

// Will be provided by the user
string XS_FILE; //Name of the cross section file (eV and b)
string IRRADIATION_FILE; //# of protons | irradiation time (h) | waiting time (h) | measuring time (h)
string SAMPLE_FILE; // Mass (gr) | Abundance | Mass Number | Atomic Mass | Element Symbol | Half life (h) |
Intensity | Efficiency 0<e<1 | Radius (cm)
string OUTPUT_FILE;
double MASS; // In g
double ABUNDANCE; // 0<A<1
double MASS_NUMBER;
double ATOMIC_MASS;
string ELEMENT;
double RADIUS; //In cm
double T_HALF_LIFE; // In h
double INTENSITY; // 0<I<1
```

```cpp
double PROTONS;
double T_WAITING; // In h
double T_MEASUREMENT; // In h
double T_IRRADIATION; // In h

// To be incorporated later
double efficiency_g; // hypothetical

//===================================
// Routine Declaration
void Read_Flux();
void Read_Irradiation_File();
void Read_Sample_File();
void Make_XS_Graph();
void Make_Flux_Histogram();
void Make_Sampling_Histogram();
double Get_Number_Of_Nuclei();
double Get_Surface(double);
double Hours_to_Seconds(double);
//==================================//
//          MAIN          //
//==================================//
int NEAR_Counts_newest_version_sg(string xs_f, string irradiation_f, string sample_f, string output_f) {
//To pass the arguements in the beginning, do NEAR_Counts_newest_version(string xs_f, string irradiation_f, string
sample_f, string output_f) {
//And comment/uncomment below as prompted
// To run, do something like root -l -b -q 'NEAR_Counts_newest_version.C("xs_114Cd.dat", "irr.dat",
"Cd_sample.dat", "Output_Cd.dat")'

  cout<<endl<<"*********************************"<<endl;

  // Uncomment if you pass them as arguements
  XS_FILE=xs_f;
  IRRADIATION_FILE=irradiation_f;
  SAMPLE_FILE=sample_f;
  OUTPUT_FILE=output_f;

  //Check if the files exist
  FileStat_t stat;
  stat.fSize=0;
  if(gSystem->GetPathInfo(XS_FILE.c_str(),stat)!=0) {cout<<endl<<"CAN'T FIND XS FILE!"<<endl; return 0;}
  if(gSystem->GetPathInfo(IRRADIATION_FILE.c_str(),stat)!=0) {cout<<endl<<"CAN'T FIND IRRADIATION
FILE!"<<endl; return 0;}
  if(gSystem->GetPathInfo(SAMPLE_FILE.c_str(),stat)!=0) {cout<<endl<<"CAN'T FIND SAMPLE
FILE!"<<endl; return 0;}
  //-------------------------------------------------

  //Read the user input files
  Read_Irradiation_File(); Read_Sample_File();

  //Fix the units and other things you need
  double t_wait = Hours_to_Seconds(T_WAITING);
  double t_irr = Hours_to_Seconds(T_IRRADIATION);
  double t_meas = Hours_to_Seconds(T_MEASUREMENT);
  double t_g = Hours_to_Seconds(T_HALF_LIFE);
  double lamda_g=log(2)/t_g; //decay constant
```

```cpp
    double nuclei=Get_Number_Of_Nuclei();

    //Read Flux File
    Read_Flux();

    //Fill and Draw the Flux Histogram
    Make_Flux_Histogram(); Make_Sampling_Histogram();
    double neutrons = Flux_Histo->Integral(1, BINS);

    //Make and Draw the Cross Section Graph
    Make_XS_Graph();

    cout<<endl<<"********************************"<<endl;


    //Check the limits of the known range (both flux and xs known)
    int from, to;
    string message1, message2;
    if (FIRST_XS_ENERGY<Flux_Histo->GetBinCenter(1)) {message1 = "> XS comes first";
cout<<endl<<message1<<endl; from=1;}
    if (FIRST_XS_ENERGY>Flux_Histo->GetBinCenter(1)) {message1="> !Flux comes first!";
cout<<endl<<message1<<endl; from=Flux_Histo->FindBin(FIRST_XS_ENERGY);}
    if (LAST_XS_ENERGY<Flux_Histo->GetBinCenter(BINS)) {message2="> We ran out of XS";
cout<<message2<<endl; to=Flux_Histo->FindBin(LAST_XS_ENERGY);}
    if (LAST_XS_ENERGY>Flux_Histo->GetBinCenter(BINS)) {message2="> We ran out of Flux";
cout<<message2<<endl; to=BINS+1;}

    //TGraph *gr = new TGraph();

    // Calculate the SACS and the total neutrons in the known range
    gRandom = new TRandom3();
    double Neutrons_With_XS=0; double a;double b;
    double sacssum=0, Neutrons_With_XS_SACS=0;
    printf("\nInitial\tOngoing\t Final bin\n");
    for (int i=from; i<to; i++) { //loop in flux histogram bins
      for (int j=0; j<NEUTRONS_FOR_SACS[i-1]; j++) { //loop in a decent number of neutrons in this bin
        sacssum += XS_Graph->Eval(gRandom->Uniform(EDGES[i-1], EDGES[i]));
      } //...loop in neutrons
      Neutrons_With_XS_SACS += NEUTRONS_FOR_SACS[i-1];
      Neutrons_With_XS += Flux_Histo->GetBinContent(i); // total neutrons/cm2
      printf("  %d\t %d\t%d\n",from, i, to);
        } //...loop in flux histogram bins

    double sacs=sacssum/Neutrons_With_XS_SACS;
    cout<<endl<<"SACS [b]: "<<sacs<<endl;
    cout<<"Neutrons with XS: "<<Neutrons_With_XS<<endl;
    cout<<"Neutrons total: "<<neutrons<<endl;
    cout<<"Ratio: "<<Neutrons_With_XS/neutrons<<endl;
    cout<<endl<<"********************************"<<endl;

    //Calculation of the total counts (ignoring the existence of any metastable states)
    double counts;
    double activity_after_irradiation, activity_after_cooling;
    double saturated_activity;
```

```cpp
counts=sacs*1e-24*Neutrons_With_XS*nuclei*INTENSITY*efficiency_g*exp(-lamda_g*t_wait)*(1-exp(-
lamda_g*t_meas))*(1-exp(-lamda_g*t_irr))/(lamda_g*t_irr);

   saturated_activity=sacs*1e-24*Neutrons_With_XS*nuclei/(t_irr);
 activity_after_irradiation=sacs*1e-24*Neutrons_With_XS*nuclei*(1-exp(-lamda_g*t_irr))/(t_irr);
 activity_after_cooling=sacs*1e-24*Neutrons_With_XS*nuclei*exp(-lamda_g*t_wait)*(1-exp(-
lamda_g*t_irr))/(t_irr);

 cout<<"Total counts (ignoring the existence of any metastable states): "<<endl<<counts<<endl;
   cout<<"Saturated activity: "<<endl<<saturated_activity<<"Bq"<<endl;
 cout<<"Activity just after irradiation: "<<endl<<activity_after_irradiation<<"Bq"<<endl;
 cout<<"Activity just after cooling: "<<endl<<activity_after_cooling<<"Bq"<<endl;
 //---------------------------------------------
 // Output results
 FILE *out;
 out = fopen(OUTPUT_FILE.c_str(), "w");
 fprintf(out, "NEAR station expected statistics for activation measurements\n\n------------------INPUT-----------------
--------\n\nSample Information\nElement:\t\0f%s\nMass:\t\t%.0f g\nAtomic Mass:\t\t%.3f\nRadius:\t\t%.2f
cm\n\nDecay information\nXS file:\t\t%s\nHalf-life:\t\t%.2f h\t%.0f s\nIntensity:\t\t%.3f\n\nIrradiation
Information\nProtons:\t\t%.1e\nNeutrons:\t\t%.4e /cm2\nIrradiation time:\t%.0f h\t%.0f s\nWaiting time:\t\t%.0f
h\t%.0f s\n\nMeasurement Information\nMeasurement time:\t%.0f h\t%.0f s\nDetector efficiency:\t%.2f\n\n\n-------
-----------RESULTS------------------------\n\nSACS\t%.3f b\nExpected counts\t%.3e\nSaturated Activity at the end of
the irradiation:\t\t%.3e Bq\nActivity at the end of the irradiation:\t\t%.3e Bq\nActivity at the end of the cooling
time:\t\t%.3e Bq\n\n\n----------------RUNTIME MESSAGES------------------\n\n%s\n%s",MASS_NUMBER,
ELEMENT.c_str(), MASS, ATOMIC_MASS, RADIUS, XS_FILE.c_str(), T_HALF_LIFE, t_g, INTENSITY,
PROTONS, neutrons, T_IRRADIATION, t_irr, T_WAITING, t_wait, T_MEASUREMENT, t_meas, efficiency_g,
sacs, counts, saturated_activity, activity_after_irradiation, activity_after_cooling, message1.c_str(),
message2.c_str());

 fclose(out);

 return 0;

}//...Main

//=================================
// Sub-Routines
void Read_Flux() {
 ifstream inFlux(FLUX_FILE);
 //cout<<endl<<"Reading Flux File"<<endl;
 int ii=0; double neutrons; double dummy; double low; double up;
 double surface=Get_Surface(RADIUS);
 while(!inFlux.eof()) {
  inFlux>>low>>up>>neutrons>>dummy;
  NEUTRONS_TOTAL[ii]=neutrons*PROTONS*(up-low); // = neutrons / cm2
  NEUTRONS_FOR_SACS[ii]=neutrons*5.e11*(up-low);
  EDGES[ii]=low*1e9; // Now in eV
  ii=ii+1;
 }
 EDGES[BINS]=up*1e9; // Now in eV
}//...Read Flux

void Read_Irradiation_File() {
 ifstream inIrr(IRRADIATION_FILE);
 FileStat_t stat;
 stat.fSize=0;
```

```
  //cout<<endl<<"Reading Irradiation File"<<endl;
  while(!inIrr.eof()) {
    inIrr>>PROTONS>>T_IRRADIATION>>T_WAITING>>T_MEASUREMENT;
  }//while
}//... Read Irradiation File

void Read_Sample_File() {
    ifstream inSample(SAMPLE_FILE);
    //cout<<endl<<"Reading Sample File"<<endl;
    while(!inSample.eof()) {

inSample>>MASS>>ABUNDANCE>>MASS_NUMBER>>ATOMIC_MASS>>ELEMENT>>T_HALF_LIFE>>I
NTENSITY>>efficiency_g>>RADIUS;
  }//...while
}//...Read Sample File

void Make_Flux_Histogram(){
  Flux_Histo  = new TH1F("Flux_Histo", "Integrated Flux Histogram", BINS, EDGES);
  for (int i=1; i<BINS+1; i++) {
    Flux_Histo->SetBinContent(i, NEUTRONS_TOTAL[i-1]);
  }//...for
  TCanvas *cf = new TCanvas("cf", "cf", 1900, 1800);
  cf->cd(); gPad->SetLogy(); gPad->SetLogx(); gStyle->SetOptStat(0);
  Flux_Histo->SetTitle("Integrated Flux Histogram;Energy (eV);Total Neutrons/cm2");
  Flux_Histo->SetLineColor(kBlack);
  Flux_Histo->SetLineWidth(2);
  Flux_Histo->Draw("HISTO][");
}//...Draw Flux Histogram

void Make_Sampling_Histogram(){
  Sampling_Histo  = new TH1F("Sampling_Histo", "Integrated Flux Histogram For Sampling", BINS, EDGES);
  for (int i=1; i<BINS+1; i++) {
    Sampling_Histo->SetBinContent(i, NEUTRONS_FOR_SACS[i-1]);
  }//...for
  TCanvas *cs = new TCanvas("cs", "cs", 1900, 1800);
  cs->cd(); gPad->SetLogy(); gPad->SetLogx(); gStyle->SetOptStat(0);
  Sampling_Histo->SetTitle("Integrated Flux Histogram For Sampling;Energy (eV);Neutrons/cm2");
  Sampling_Histo->SetLineColor(kBlack);
  Sampling_Histo->SetLineWidth(2);
  Sampling_Histo->Draw("HISTO][");
}//...Draw Flux Histogram to be used for sampling

void Make_XS_Graph() {
  ifstream inXS(XS_FILE);
  double energy, xs;
  int ii=0;
  while(!inXS.eof()) {
    inXS>>energy>>xs;
    XS_Graph->SetPoint(ii, energy, xs);
    ii=ii+1;
  }//...while
  double dummy;
  XS_Graph->GetPoint(0, FIRST_XS_ENERGY, dummy);
  LAST_XS_ENERGY = energy;
  TCanvas *cx = new TCanvas("cx", "cx", 1900, 1800);
  cx->cd(); gPad->SetLogx(); gPad->SetLogy();
```

```
  XS_Graph->SetMarkerStyle(20);
  XS_Graph->SetMarkerSize(0.5);
  XS_Graph->SetMarkerColor(kBlack);
  XS_Graph->SetTitle("Cross Section;Energy (eV);Cross Section (b)");
  XS_Graph->Draw("AP");
}//...Make Cross Section Graph

double Get_Number_Of_Nuclei() {
  double nuclei;
  nuclei = MASS * ABUNDANCE * AVOGADRO / ATOMIC_MASS;
  return nuclei;
}//...Get Number Of Nuclei

double Get_Surface(double r) {
  double surface;
  surface = PI * RADIUS * RADIUS;
  return surface;
}//...Get Sample Surface

double Hours_to_Seconds(double h) {
  double s;
  s = h * 60 * 60;
  return s;
}//...Hours to Seconds
```

E

GEANT4 SIMULATIONS

Monte-Carlo Simulations code based on GEANT4 for the estimation of the accurate gamma-ray detection [1].

---

[1]Basic Author: Elisso Stamati, Developer: Styliani Goula

```cpp
//  GEM80

#include "XriDetectorConstruction.hh"
#include "G4SDManager.hh"
#include "G4Element.hh"
#include "G4Material.hh"
#include "G4Box.hh"
#include "G4Tubs.hh"
#include "G4LogicalVolume.hh"
#include "G4ThreeVector.hh"
#include "G4PVPlacement.hh"

#include "G4UnitsTable.hh"
#include "globals.hh"

#include "G4VisAttributes.hh"
#include "G4Colour.hh"


#include "G4SystemOfUnits.hh"
#include "G4PhysicalConstants.hh"

#include "G4NistManager.hh"

XriDetectorConstruction::XriDetectorConstruction()
{;}

XriDetectorConstruction::~XriDetectorConstruction()
{;}

G4VPhysicalVolume* XriDetectorConstruction::Construct()
{

  G4UnitDefinition::BuildUnitsTable();

      //============================= materials =====================================//

  G4double a;
  G4double z;
  G4int iz, in;
  G4double density;
  G4String name, symbol;
  G4int ncomponents;
  G4double fractionmass;
  G4int natoms;

  //------ Plexiglass of the source // Let's use this for the Cs source

  a = 12.011*g/mole;
  G4Element* elC = new G4Element(name="Carbon",symbol=" C", z=6., a);

  a = 1.008*g/mole;
  G4Element *elH  = new G4Element(name="Hydrogen",  symbol=" H" , z= 1., a);

  a = 15.999*g/mole;
  G4Element *elO  = new G4Element(name="Oxygen",  symbol=" O" , z= 8., a);
```

```cpp
a = 14.007*g/mole;
G4Element *elN  = new G4Element(name="Nitrogen",  symbol="N" , z= 7., a);

a = 26.981539*g/mole;
G4Element *elAl  = new G4Element(name="Aluminium",  symbol="Al" , z= 13., a);

a = 58.933194*g/mole;
G4Element *elCo  = new G4Element(name="Cobalt",  symbol="Co" , z= 27., a);

a = 114.818*g/mole;
G4Element *elIn  = new G4Element(name="Indium",  symbol="In" , z= 49., a);

a = 58.6934*g/mole;
G4Element *elNi  = new G4Element(name="Nickel",  symbol="Ni" , z= 28., a);

a = 208.9804*g/mole;
G4Element *elBi  = new G4Element(name="Bismuth",  symbol="Bi" , z= 83., a);

a=183.84*g/mole;
G4Element *elW  = new G4Element(name="Tungsten",  symbol="W" , z= 74., a);

a=112.411*g/mole;
G4Element *elCd  = new G4Element(name="Cadmium",  symbol="Cd" , z= 48., a);

// ------- defining Ge crystal

a = 72.61*g/mole;
density = 5.323*g/cm3;
G4Material* Ge = new G4Material(name="Ge",z=32., a, density);

// ------- defining Al foil and housing

a = 26.981539*g/mole;
density = 2.70*g/cm3;
G4Material* Al = new G4Material(name="Al", z=13., a, density);

// -------- defying iron
a = 55.845*g/mole;
density = 7.874*g/cm3;
G4Material* Fe = new G4Material(name="Fe", z=26., a, density);

 // -------- defying gold
 a=196.966569*g/mole;
 density = 19.3*g/cm3;
 G4Material* Au = new G4Material(name="Au", z=79., a, density);

 // -------- defying cobalt
 a = 58.933194*g/mole;
 density = 8.9*g/cm3;
 G4Material* Co = new G4Material(name="Co",z=27., a, density);

 // -------- defying Bismuth
 a = 208.9804*g/mole;
 density = 9.8*g/cm3;
 G4Material* Bi = new G4Material(name="Bi",z=83., a, density);
```

```cpp
// -------- defying indium
a = 114.818*g/mole;
density = 7.3*g/cm3;
G4Material* In = new G4Material(name="In",z=49., a, density);

// -------- defying nickel
a = 58.6934*g/mole;
density = 8.9*g/cm3;
G4Material* Ni = new G4Material(name="Ni",z=28., a, density);

// -------- defying tungsten
a=183.84*g/mole;
density = 19.3*g/cm3;
G4Material* W = new G4Material(name="W", z=74., a, density);

// -------- defying Cadmium
a=112.411*g/mole;
density = 19.3*g/cm3;
G4Material* Cd = new G4Material(name="Cd", z=48., a, density);


// ------- Mylar

density = 1.39*g/cm3;
G4Material *Mylar = new G4Material(name="Mylar", density, ncomponents=3);
Mylar->AddElement(elO, natoms=2);
Mylar->AddElement(elH, natoms=4);
Mylar->AddElement(elC, natoms=5);

// ----------Kapton // Let's use this for the Eu source

density = 1.413*g/cm3;
G4Material* Kapton = new G4Material(name="Kapton", density, ncomponents=4);
Kapton->AddElement(elO, natoms=5);
Kapton->AddElement(elC, natoms=22);
Kapton->AddElement(elN, natoms=2);
Kapton->AddElement(elH, natoms=10);

//-----------Aliminium salt

density =3.95*g/cm3;
G4Material* Al_salt = new G4Material(name="Al_salt", density, ncomponents=2);
Al_salt->AddElement(elO,natoms=3);
Al_salt->AddElement(elAl,natoms=2);

//---------- Defining Air

density = 1.29*mg/cm3;
G4Material *Air = new G4Material(name="Air ",density,ncomponents=2);
Air->AddElement(elO, fractionmass=30.0*perCent);
Air->AddElement(elN, fractionmass=70.0*perCent);

// -----   defining vacuum

G4double pressure, temperature;
```

```
density = universe_mean_density;
pressure = 3.0E-18*pascal;
temperature = 2.73*kelvin;
G4Material *Vacuum = new G4Material(name="Vacuum", z=1.0, a=1.01*g/mole,
                    density, kStateGas, temperature, pressure);



G4cout << "\n\n ####-------------------------------------------------------#### \n";
G4cout << "\n\t\t#### List of isotopes used #### \n";
//  G4cout << *(G4Isotope::GetIsotopeTable());
G4cout << "\n\n\n\t\t #### List of elements used #### \n";
G4cout << *(G4Element::GetElementTable());
G4cout << "\n\n\n\t\t #### List of materials used #### \n";
G4cout << *(G4Material::GetMaterialTable());
G4cout << "\n\n ####-------------------------------------------------------#### \n";



//================================ volumes ==============================//

//---------------------------- beam line along z axis

G4double startFi = 0.0*deg;
G4double endFi = 360.0*deg;

//---------------------------- world volume

G4double WorldOutR = 20.0*cm;
G4double WorldInR = 0.0*cm;
G4double WorldHalfh = 30.0*cm;

G4Tubs *World_tub
  = new G4Tubs("World_tub",WorldInR,WorldOutR,WorldHalfh,
                        startFi,endFi);

G4LogicalVolume *World_log
  = new G4LogicalVolume(World_tub,Air,"World_log",0,0,0);

G4VPhysicalVolume *World_phys
  = new G4PVPlacement(0,G4ThreeVector(),"World",
              World_log,0,false,0);

// Target:
G4double TargetOutR = 0.65*cm;
G4double TargetInR = 0.*cm;
G4double TargetHalfh = 0.1/2*cm;

G4Tubs *Target_tube = new G4Tubs("Target_tube", TargetInR, TargetOutR, TargetHalfh, startFi, endFi);
G4LogicalVolume *Target_log = new G4LogicalVolume(Target_tube, Cd , "Target_log", 0, 0, 0);

G4double Pos_x = 0.0*cm;
G4double Pos_y = 0.0*cm;
G4double Pos_z = 0.0*cm;

G4VPhysicalVolume *TargetTube_phys
  = new G4PVPlacement(0,
              G4ThreeVector(Pos_z, Pos_y, Pos_z),
```

```
                    Target_log, "TargetTube", World_log, false, 0);


G4double SD = 9.0*cm; //source detector distance: Active surface to detector window

G4double AlOutR = 4.0*cm;
G4double AlInR = 0;
G4double AlHalfh = 6.8*cm;
G4double AlThickness =0.15*cm;

G4Tubs *Al_tube
  = new G4Tubs("Al_tube",AlInR,AlOutR,AlHalfh,startFi,endFi);


G4LogicalVolume *Al_log
  = new G4LogicalVolume(Al_tube,Al,"Al_log",0,0,0);

Pos_x = 0.0*cm;
Pos_y = 0.0*cm;
Pos_z = -SD-AlHalfh;
G4VPhysicalVolume *AlTube_phys
  = new G4PVPlacement(0,
                G4ThreeVector(Pos_x,Pos_y,Pos_z),
                Al_log,"AlTube",World_log,false,0);

//-------------- Vacuum between housing and crystal

G4double VacuumOutR = AlOutR - AlThickness;
G4double VacuumInR = 0.*cm;
G4double VacuumHalfh = AlHalfh - AlThickness;

G4Tubs *Vacuum_tube
  = new G4Tubs("Vacuum_tube",VacuumInR,VacuumOutR,VacuumHalfh,
        startFi,endFi);

G4LogicalVolume *Vacuum_log
  = new G4LogicalVolume(Vacuum_tube,Vacuum,"Vacuum_log",0,0,0);

Pos_x = 0.0*cm;
Pos_y = 0.0*cm;
Pos_z = 0.0*cm;
G4VPhysicalVolume *VacuumTube_phys
  = new G4PVPlacement(0,
                G4ThreeVector(Pos_x,Pos_y,Pos_z),
        Vacuum_log,"VacuumTube",Al_log,false,0);

//-------------- Dead layer of crystal entrance and crystal sides: denoted as "outDead"

G4double gap = 0.59*cm;   // Distance from the back face of Al window to front dead layer face of crystal
// nTOF prototype manufacturer = 0.45*cm
G4double GeOutR = 5.32/2.0*cm;
// nTOF prototype manufacturer = 5.8/2
G4double GeHalfh= 4.96/2.0*cm;
// nTOF prototype manufacturer = 5.1/2
G4double outDeadThickness = 0.17*cm;
// nTOF prototype manufacturer = 0.05
```

```
G4double outDeadOutR = GeOutR + outDeadThickness;
G4double outDeadInR = 0.*mm;
G4double outDeadHalfh = GeHalfh +outDeadThickness/2.;

G4Tubs *outDead_tube
  = new G4Tubs("outDead_tube",outDeadInR,outDeadOutR,outDeadHalfh,
        startFi,endFi);

G4LogicalVolume *outDead_log
  = new G4LogicalVolume(outDead_tube,Ge,"outDead_log",0,0,0);

Pos_x = 0.0*cm;
Pos_y = 0.0*cm;
Pos_z = VacuumHalfh - outDeadHalfh - gap;
G4VPhysicalVolume *outDeadTube_phys
  = new G4PVPlacement(0,
               G4ThreeVector(Pos_x,Pos_y,Pos_z),
        outDead_log,"outDeadTube",Vacuum_log,false,0);


//------------------ Ge crystal

G4double GeInR = 0.*mm;

G4Tubs *Ge_tube
  = new G4Tubs("Ge_tube",GeInR,GeOutR,GeHalfh,
        startFi,endFi);

G4LogicalVolume *Ge_log
  = new G4LogicalVolume(Ge_tube,Ge,"Ge_log",0,0,0);

Pos_x = 0.0*cm;
Pos_y = 0.0*cm;
Pos_z = - outDeadThickness/2.;

G4VPhysicalVolume *GeTube_phys
  = new G4PVPlacement(0,
        G4ThreeVector(Pos_x,Pos_y,Pos_z),
        Ge_log,"GeTube",outDead_log,false,0);

//----------- Dead layer in borehole: denoted as inDead

G4double BoreholeHalfh = 2.44/2.*cm;
G4double BoreholeOutR = 0.5*cm;


//--------------- Borehole

G4double BoreholeInR = 0.*mm;

G4Tubs *Borehole_tube
  = new G4Tubs("Borehole_tube",BoreholeInR,BoreholeOutR,BoreholeHalfh,
                    startFi,endFi);

G4LogicalVolume *Borehole_log
```

```
       = new G4LogicalVolume(Borehole_tube,Vacuum,"Borehole_log",0,0,0);

   Pos_x = 0.0*cm;
   Pos_y = 0.0*cm;
   Pos_z = -GeHalfh + BoreholeHalfh; //- inDeadThickness/2.;
   G4VPhysicalVolume *BoreholeTube_phys
     = new G4PVPlacement(0,
           G4ThreeVector(Pos_x,Pos_y,Pos_z),
                    Borehole_log,"BoreholeTube",Ge_log,false,0);//inDead_log,false,0);


       //========================== Visualization attributes
   ==========================================//

   World_log->SetVisAttributes (G4VisAttributes::Invisible);
   G4VisAttributes *AlTubeAttr = new G4VisAttributes(G4Colour(1.,0.,0.));        //Red
   G4VisAttributes *VacuumTubeAttr = new G4VisAttributes(G4Colour(0.3,0.3,0.3)); //light gray
   G4VisAttributes *outDeadTubeAttr = new G4VisAttributes(G4Colour(1.,0.,0.));   //red
   G4VisAttributes *GeTubeAttr = new G4VisAttributes(G4Colour(0.8,0.8,0.8));     //grey
   G4VisAttributes *BoreholeTubeAttr = new G4VisAttributes(G4Colour(0.,0.,1.));  //blue

   G4VisAttributes *MylarTubeAttr = new G4VisAttributes(G4Colour(0.0,0.0,0.0));  //black
   //G4VisAttributes *TargetTubeAttr = new G4VisAttributes(G4Colour(1.,0.,1.)); // magenta
   G4VisAttributes *Al_frontTubeAttr = new G4VisAttributes(G4Colour(0.0,0.0,1.)); // blue


   VacuumTubeAttr->SetVisibility(true);
   VacuumTubeAttr->SetForceWireframe(true);
   Vacuum_log->SetVisAttributes(VacuumTubeAttr);

   outDeadTubeAttr->SetVisibility(true);
   outDeadTubeAttr->SetForceWireframe(true);
   outDead_log->SetVisAttributes(outDeadTubeAttr);

   GeTubeAttr->SetVisibility(true);
   GeTubeAttr->SetForceWireframe(true);
   Ge_log->SetVisAttributes(GeTubeAttr);


   BoreholeTubeAttr->SetVisibility(true);
   BoreholeTubeAttr->SetForceWireframe(true);
   Borehole_log->SetVisAttributes(BoreholeTubeAttr);

   //MylarTubeAttr->SetVisibility(true);
   //MylarTubeAttr->SetForceWireframe(true);
   //Mylar_log->SetVisAttributes(MylarTubeAttr);
   /*

   TargetTubeAttr->SetVisibility(true);
   TargetTubeAttr->SetForceWireframe(true);
   Target_log->SetVisAttributes(TargetTubeAttr);*/

   //Al_frontTubeAttr->SetVisibility(true);
   //Al_frontTubeAttr->SetForceWireframe(true);
   //Al_front_log->SetVisAttributes(Al_frontTubeAttr);
```

```
AlTubeAttr->SetVisibility(true);
AlTubeAttr->SetForceWireframe(true);
Al_log->SetVisAttributes(AlTubeAttr);


return World_phys;
}
```

```cpp
#include "XriPrimaryGeneratorAction.hh"

#include "G4RunManager.hh"
#include "G4Event.hh"
#include "G4ParticleGun.hh"
#include "G4ParticleTable.hh"
#include "G4IonTable.hh"
#include "G4ParticleDefinition.hh"
#include "G4ChargedGeantino.hh"
#include "G4SystemOfUnits.hh"
#include "Randomize.hh"

#include "G4SystemOfUnits.hh"
#include "G4PhysicalConstants.hh"

//....oooOO0OOooo........oooOO0OOooo........oooOO0OOooo........oooOO0OOooo......

XriPrimaryGeneratorAction::XriPrimaryGeneratorAction()
 : G4VUserPrimaryGeneratorAction(),
   fParticleGun(0)
{
  G4int n_particle = 1;
  fParticleGun  = new G4ParticleGun(n_particle);

  G4ParticleTable* particleTable = G4ParticleTable::GetParticleTable();
  G4ParticleDefinition* particle
              = particleTable->FindParticle("chargedgeantino");
  fParticleGun->SetParticleDefinition(particle);
  fParticleGun->SetParticlePosition(G4ThreeVector(0.,0.,0.));
  fParticleGun->SetParticleEnergy(1*eV);
  fParticleGun->SetParticleMomentumDirection(G4ThreeVector(1.,0.,0.));
}

//....oooOO0OOooo........oooOO0OOooo........oooOO0OOooo........oooOO0OOooo......

XriPrimaryGeneratorAction::~XriPrimaryGeneratorAction()
{
  delete fParticleGun;
}

//....oooOO0OOooo........oooOO0OOooo........oooOO0OOooo........oooOO0OOooo......

void XriPrimaryGeneratorAction::GeneratePrimaries(G4Event* anEvent)
{
  G4ParticleDefinition* particle = fParticleGun->GetParticleDefinition();
  if (particle == G4ChargedGeantino::ChargedGeantino()) {
    //fluorine
    G4int Z =49, A =114 ;
    G4double ionCharge   = 0.*eplus;
    G4double excitEnergy = 190.23*keV;

  G4ParticleDefinition* ion
     = G4IonTable::GetIonTable()->GetIon(Z,A,excitEnergy);

    fParticleGun->SetParticleDefinition(ion);
    fParticleGun->SetParticleCharge(ionCharge);
```

```
  }
  //----------------------------------------------------------------
G4double px0=0., py0=0., pz0=0.;

G4double Pi =3.14159;
  G4double  phi= 2.*Pi* G4UniformRand();

  G4double cosTheta = -1. + 2. * G4UniformRand();
  G4double sinTheta = sqrt(1. - cosTheta * cosTheta);

  px0= sinTheta * cos(phi);
  py0= sinTheta * sin(phi);
  pz0 =cosTheta;

  fParticleGun->SetParticleMomentumDirection(G4ThreeVector(px0, py0, pz0));
  //----------------------------------------------------------------

  G4double x0  = 0.*cm, y0  = 0.*cm, z0  = 0.*cm;

  G4double rho=0.3/2.*cm;
  G4double dz0 = 0.05*cm;

  back:
  x0 = rho*(1.-2.*G4UniformRand());
  y0 = rho*(1.-2.*G4UniformRand());
  if ((x0*x0+y0*y0)>(rho*rho)) goto back;
  z0 = dz0*(G4UniformRand()-0.5);

  fParticleGun->SetParticlePosition(G4ThreeVector(x0,y0,z0));

  fParticleGun->GeneratePrimaryVertex(anEvent);

}

//....oooOO0OOooo........oooOO0OOooo........oooOO0OOooo........oooOO0OOooo......
```

F

MEASUREMENT PLAN

On the following pages you will find the exact measurement schedule that took place in n_TOF's Electronics Laboratory. The measurements started from 20/10 until 8/11 when all the samples were measured two to three times, when of course this was possible. Then, long-lasting measurements were performed to obtain background spectra.

Table F.1: Actual Measurement Plan

Sample	Diameter [mm]	Reaction	E_g [KeV]	Intensity [%]	SD [cm]	Start	End
20/10/21							
Ni	13	58Ni (n, p) 58Co	810,775	99,000	9	20/10/21 15:19	20/10/21 17:17
		58Ni (n, 2n) 57Ni	1377,63	81,7			
W	13	186W (n, g) 187W	685,774	27,3	12	20/10/21 17:28	20/10/21 17:34
Al	13	27Al (n, a) 24Na	1368.633	100	9	20/10/21 17:39	20/10/21 20:35
Cd	13	114Cd (n, g) 115Cd	527,900	27,450	9	20/10/21 20:45	20/10/21 20:53
Bi	13	209Bi (n,3n) 207Bi	1063,662	74,5	9	20/10/21 20:55	21/10/21 09:46
		209Bi (n, 4n) 206Bi	803,100	99			
		209Bi (n, 5n) 205Bi	1764,36	32,5			
21/10/21							
Au3	3	back	197Au (n, g) 198Au	411,802	96,000	9	21/10/21 10:00	21/10/21 16:10
		197Au (n, 2n) 196Au	355,684	87,000			
W	13	186W (n, g) 187W	685,774		12	21/10/21 16:47	21/10/21 16:50
Cd	13	114Cd (n, g) 115Cd	527,900		9	21/10/21 16:54	21/10/21 17:05
Au6	13	back	197Au (n, 2n) 196Au	355,684	87,000	12	21/10/21 17:09	21/10/21 20:20

84

Sample	Position	Reaction	Energy	Abundance	Time	Start	End
Au4	3 | back	197Au (n, g) 198Au	411,802	96,000	9	21/10/21 20:37	22/10/21 10:26
		197Au (n, 2n) 196Au	355,684	87,000			
22/10/21							
Aub	3	197Au (n, g) 198Au	411,802	96,000	9	22/10/21 10:42	22/10/21 18:36
		197Au (n, 2n) 196Au	355,684	87,000			
Au6	13 | back	197Au (n, 2n) 196Au	355,648		12	22/10/21 18:52	22/10/21 19:04
Au1	3 | front	197Au (n, g) 198Au	411,802	96,000	12	22/10/21 19:11	24/10/21 18:10
		197Au (n, 2n) 196Au	355,684	87,000			
		197Au (n, 4n) 194Au	328,455	61,000			
24/10/21							
In	13	113In (n, g) 114In m	190,29	15,56	9	24/10/21 18:20	24/10/21 18:43
Au2	3 | front	197Au (n, g) 198Au	411,802		12	24/10/21 18:50	25/10/21 14:53
		197Au (n, 2n) 196Au	355,684				
		197Au (n, 4n) 194Au	328,455				
25/10/21							
Sc	3	45Sc (n, g) 46Sc	1120,545	99,987	9	25/10/21 15:01	25/10/21 17:13
Co	3	59Co (n, g) 60Co	1332,501	99,9856	9	25/10/21 17:25	27/10/21 10:53
		59Co (n, 2n) 58Co	810,775	99			
		59Co (n, 3n) 57Co	122,0614	85,6			

27/10/21

Sc	3	45Sc (n, g) 46Sc	1120,545	9	27/10/21 11:05	25/10/21 16:02
Ni	13	58Ni (n, p) 58Co	810,775	9	27/10/21 16:14	27/10/21 16:48
In	13	113In (n, g) 114In m	190,29	9	27/10/21 16:50	27/10/21 17:16
Au1	3 l front	197Au (n, g) 198Au	411,802	12	27/10/21 17:48	28/10/21 15:39
		197Au (n, 2n) 196Au	355,684			
		197Au (n,3n) 195Au	98,85			
		197Au (n, 4n) 194Au	328,455			

28/10/21

Au1	3 l front	197Au (n,3n) 195Au	98,85	3	28/10/21 15:43	28/10/21 17:25
Bi	13	209Bi (n,3n) 207Bi	1063,662	9	28/10/21 17:27	29/10/21 12:29
		209Bi (n, 4n) 206Bi	803,100			
		209Bi (n, 5n) 205Bi	1764,36			

29/10/21

Au1	3 l front	197Au (n, g) 198Au	411,802	3	29/10/21 12:47	1/11/2021 ~18:05
		197Au (n, 2n) 196Au	355,684			
		197Au (n,3n) 195Au	98,85			
		197Au (n, 4n) 194Au	328,455			

1/11/21

Sample		Reaction	Energy		Date/Time 1	Date/Time 2
Co	3	59Co (n, g) 60Co	1332,501	9	1/11/21 17:49	2/11/21 15:34
		59Co (n, 2n) 58Co	810,775			
		59Co (n, 3n) 57Co	122,0614			
2/11/21						
152 Eu	-	-	-	3	2/11/21 15:54	2/11/21 16:20
152 Eu	-	-	-	12	2/11/21 16:22	3/11/21 11:36
3/11/21						
152 Eu	-	-	-	12	3/11/21 11:39	3/11/21 14:44
Bi	13	209Bi (n,3n) 207Bi	1063,662	9	3/11/21 16:05	4/11/21 14:55
		209Bi (n, 4n) 206Bi	803,100			
		209Bi (n, 5n) 205Bi	1764,36			
4/11/21						
Au3	3 l back	197Au (n, g) 198Au	411,802	9	4/11/21 15:42	5/11/21 11:28
		197Au (n, 2n) 196Au	355,684			
5/11/21						
Aub	3	197Au (n, g) 198Au	411,802	9	5/11/21 11:45	6/11/21 12:24
		197Au (n, 2n) 196Au	355,684			
6/11/21						
Au4	3 l back	197Au (n, g) 198Au	411,802	9	6/11/21 12:33	7/11/21 14:43

Date	Sample	#	Position	Reaction	Counts		Start	End
				197Au (n, 2n) 196Au	355,684			
7/11/21								
	Au6	13	back	197Au (n, 2n) 196Au	355,648	12	7/11/21 14:49	8/11/21 12:17
8/11/21								
	Au2	3	front	197Au (n, g) 198Au	411,802	12	8/11/21 12:24	9/11/21 14:43
				197Au (n, 2n) 196Au	355,684			
				197Au (n, 4n) 194Au	328,455			

[1] J. Bond, D. Lauretta, C. Tinney, R. Butler, G. Marcy, H. Jones, B. Carter, S. O'Toole, and J. Bailey, "Beyond the iron peak: r-and s-process elemental abundances in stars with planets," *The Astrophysical Journal*, vol. 682, no. 2, p. 1234, 2008.

[2] Y. Kadi and J. Revol, "Design of an accelerator-driven system for the destruction of nuclear waste, https://inis.iaea.org/collection/nclcollectionstore/public/38/071/38071996.pdf," 2003.

[3] D. A. Brown, M. Chadwick, R. Capote, A. Kahler, A. Trkov, M. Herman, A. Sonzogni, Y. Danon, A. Carlson, M. Dunn, *et al.*, "Endf/b-viii. 0: The 8th major release of the nuclear reaction data library with cielo-project cross sections, new standards and thermal scattering data," *Nuclear Data Sheets*, vol. 148, pp. 1–142, 2018.

[4] "JENDL: Japan evaluated nuclear data library," *https://wwwndc.jaea.go.jp/jendl/j5/j5.html*.

[5] "JEFF: Joint evaluated fission and fusion nuclear data library," *https://www.oecd-nea.org/dbdata/jeff/*.

[6] "BROND: Russian evaluated neutron data library," *https://inis.iaea.org/search/search.aspx?orig$_q$ = RN : 24040171*.

[7] "CENDL: Chinese evaluated nuclear data library," *https://en.cnnc.com.cn/2020-06/17/c$_5$01119.htm*.

[8] "TENDL: Talys-based evaluated nuclear data," *https://tendl.web.psi.ch/tendl_2019/tendl2019.html*.

[9] *n_TOF: The neutron Time-Of-Flight facility at CERN, https://ntof-exp.web.cern.ch*.

[10] D. Chiesa, M. Carta, V. Fabrizio, L. Falconi, A. Grossi, M. Nastasi, M. Palomba, S. Pozzi, E. Previtali, P. G. Rancoita, *et al.*, "Characterization of triga rc-1 neutron irradiation facilities for radiation damage testing," *The European Physical Journal Plus*, vol. 135, no. 4, p. 349, 2020.

[11] C. Rubbia, A. Tzima, Y. Kadi, S. A. Andriamonje, I. Goulas, R. Cappi, S. Buono, J. P. C. Revol, P. Cennini, D. Bouvet-Bensimon, *et al.*, "A high resolution spallation driven facility at

the cern-ps to measure neutron cross sections in the interval from 1 ev to 250 mev: a relative performance assessment," tech. rep., 1998.

[12] F. Gunsing, O. Aberle, J. Andrzejewski, L. Audouin, V. Bécares, M. Bacak, J. Balibrea-Correa, M. Barbagallo, S. Barros, F. Bečvář, *et al.*, "Nuclear data activities at the n_tof facility at cern," *The European Physical Journal Plus*, vol. 131, no. 10, pp. 1–13, 2016.

[13] E. Chiaveri, O. Aberle, V. Alcayne, S. Amaducci, J. Andrzejewski, L. Audouin, V. Babiano-Suarez, M. Bacak, M. Barbagallo, S. Bennett, *et al.*, "Status and perspectives of the neutron time-of-flight facility n_tof at cern," in *EPJ Web of Conferences*, vol. 239, p. 17001, EDP Sciences, 2020.

[14] S. Goula, N. Patronis *et al.*, "Near at n_tof/cern: Preparing the first multi-foil activation measurement," *Proceedings of the 23rd Hellenic Symposium on Nuclear Physics*, 2021.

[15] G. Collaboration, *GEANT4: A simulation toolkit - Book For Application Developers, Release 10.7, 2020.*

[16] M. N. H. Comsan, "Spallation neutron sources for science and technology," *Proceedings of the 8th Conference on Nuclear and Particle Physics*, 2014.

[17] M. Barbagallo, C. Guerrero, A. Tsinganis, D. Tarrio, S. Altstadt, S. Andriamonje, J. Andrzejewski, L. Audouin, V. Bécares, F. Bečvář, *et al.*, "High-accuracy determination of the neutron flux at n_tof," *The European Physical Journal A*, vol. 49, no. 12, pp. 1–11, 2013.

[18] M. Sabaté-Gilarte, M. Barbagallo, N. Colonna, F. Gunsing, P. Žugec, V. Vlachoudis, Y. Chen, A. Stamatopoulos, J. Lerendegui-Marco, M. Cortés-Giraldo, *et al.*, "High-accuracy determination of the neutron flux in the new experimental area n_tof-ear2 at cern," *The European Physical Journal A*, vol. 53, no. 10, pp. 1–13, 2017.

[19] R. Esposito, A. Perillo-Marcone, V. Vlachoudis, R. Logé, V. Maire, P. Moyret, A. T. P. Fontenla, K. Kershaw, D. Grenier, N. Colonna, *et al.*, "arxiv: Design of the third-generation lead-based neutron spallation target for the n_tof facility at the european laboratory for particle physics," tech. rep., 2021.

[20] n_TOF Collaboration, "The new n_tof near station," 2020.

[21] *FLUKA Monte Carlo Simulation package, http://www.fluka.org/fluka.php.*

[22] M. Barbagallo, "Report on fluka simulations, near working group meeting," 2021.

[23] B. Zohuri, *Neutronic analysis for nuclear reactor systems*.
Springer, 2017.

[24] K. S. Krane, "Introductory nuclear physics," *Physics Today*, vol. 42, no. 1, p. 78, 1989.

[25] W. D. Ehmann and D. E. Vance, "Radiochemistry and nuclear methods of analysis," 1993.

[26] N. Tsoulfanidis and S. Landsberger, *Measurement & detection of radiation*. CRC press, 2021.

[27] G. Gilmore, J. Hemingway, and J. Durell, "Practical gamma-ray spectroscopy," *Journal of Physics G-Nuclear and Particle Physics*, vol. 22, no. 7, p. 1117, 1996.

[28] K. Debertin and R. G. Helmer, "Gamma-and x-ray spectrometry with semiconductor detectors," 1988.

[29] G. F. Knoll, *Radiation detection and measurement*. John Wiley & Sons, 2010.

[30] S. Usman and A. Patil, "Radiation detector deadtime and pile up: A review of the status of science," *Nuclear Engineering and Technology*, vol. 50, no. 7, pp. 1006–1016, 2018.

[31] M. D. Glascock, "An overview of neutron activation analysis," *Columbia, MO: University of Missouri Research Reactor (MURR)*, 2006.

[32] *National Nuclear Data Center, Brookhaven National Laboratory, USA.* https://www.nndc.bnl.gov.

[33] *ROOT Data Analysis Framework, User's Guide.* https://root.cern.ch/root/htmldoc/guides/users-guide/ROOTUsersGuideA4.pdf, 2020.

[34] M. E. Stamati, "Feasibility study for neutron inelastic cross section measurements at n_tof/cern using hpge detectors," 2020, unpublished.